High Cycle Rotating Bending Fatigue of 6061-T6 Friction Stir Welded Extrusions

A Senior Project
Presented to
The Faculty of the Materials Engineering Department
California Polytechnic State University, San Luis Obispo

In Partial Fulfillment
of the Requirements for the Degree
Bachelor of Science

by

John Chang

and

Travis Miller

June, 2014

Table of Contents

List of Figures

List of Tables

Acknowledgements

We would like to thank Sapa for sponsoring our senior project. For giving us funding and providing the materials needed for testing. Without their dedication to the Cal Poly Materials Engineering Department this project would not have been possible. We would like to thank Ken Fischer for his guidance and his advice throughout the entire project, and Mike Tozier for his support and time taken to visit us at the technical conference. Finally we would like to thank our advisor Dr. Blair London for his continued support and dedication to us as students as well as helping us with this project. For his guidance and advice throughout the year, and for teaching us the skills needed to be an asset in the technical community.

Abstract

Fatigue testing was done on friction stir welded joints of 6061-T6 aluminum extrusions. Tests were run using a rotating bending fatigue machine at stresses from 111.5 to 138.7 MPa. Failures occurred on the order of 10^5 to 10^7 cycles, and an S-N curve was generated based off of the failure results. After the samples failed, the location of the failure and the number of cycles to failure were noted. Fatigue samples were designed in SolidWorks with a tapered 2 inch reduced section. The 2 inch reduced section will include the entire weld region as seen from the microhardness profile of the weld, and the taper allows the aluminum samples to have equal stress along the surface of the sample across the reduced section, allowing fatigue to target the weakest area of the joint. Strain gauge testing was done to prove the model, which states that the reduced section was under equal stress. There was only a 1 MPa difference when comparing the stresses on either side of the weld. The strain gauge testing was also used to convert the applied moment that is set on the RBF machine into a stress value that will be used in the S-N curve. Fatigue strength for both the base metal and the FSW samples were higher than that stated in the literature. Micrographs were taken to find the location and grain structure of where failure occurred in the samples. SEM analysis was done on samples that failed at a low number of cycles to check for abnormalities in the material and find reasons for premature failure. The friction stir welded aluminum had failures on both sides of the stir zone between the heat affected zone and thermal mechanical affected zone.

Key Words: Materials Engineering, Friction Stir Welding, Bobbin Tool, 6061-T6, Aluminum, Extrusion, Fatigue, Rotating Bending Fatigue, Sapa

1 Introduction

1.1 Applications

Bobbin tool friction stir welded aluminum is still a growing area of research. It is currently used in the transportation and aerospace industry, shipbuilding and marine industry, and construction for bridges and pipes, as well as electrical and gas [1].

1.2 Aluminum Alloys (6061)

Aluminum is the third most abundant element in the earth's crust. It is found in the form of bauxite and smelted into its pure metallic state. It is light weight, ductile, has good thermal and electrical conductivity, and high specific strength when alloyed. It forms a face centered cubic (FCC) structure with many slip systems, making it ductile. When alloyed with elements such as magnesium (Mg) and silicon (Si), specific properties of aluminum can be optimized for a variety of high strength applications. 6061 is a 6xxx series aluminum alloy with Si and Mg as the main alloying elements (Table I). It is a heat treatable aluminum alloy meaning that it can be age hardened when a homogenized supersaturated aluminum is heated to promote precipitation. The aging process will give the alloy more strength. Aluminum alloy 6061 is one of the most commonly used aluminum alloys. Its formability, weldability, corrosion resistance, high specific strength and modulus, and relatively low cost make it ideal for structural applications, pipelines, marine applications, and transportation. The material properties of 6061 aluminum in the T6 heat treated condition are presented in Table II.

Table I: Alloying Elements Added to 6061-T6 Aluminum Alloys [2].

Si	Fe	Cu	Mn	Mg	Cr	Zn	Ti
0.4-0.8	0.7 Max	0.15-0.4	0.15 Max	0.8-1.2	0.04-0.35	0.25 Max	0.15 Max

Table II: Mechanical Properties of 6061-T6 Aluminum Alloy [3].

Properties	Value
Young's Modulus	69.8 GPa
Tensile Strength	278 MPa
Yield Strength	237 MPa
Hardness-Vickers	99.9 HV
Fatigue Strength at 10^7 cycles	94.9 MPa

The addition of Mg and Si to aluminum forms the FCC compound Mg_2Si (β) which gives the 6xxx series its heat treatability [4]. Other alloying elements also affect the properties of 6061 aluminum. Small amounts of Cu or Zn improve strength with little loss in corrosion resistance, while V, Zr, and Ti control the grain size. Sometimes Pb and Bi are added for improved machinability [5]. There are four equilibrium phases of Al-Mg-Si alloys. These phases are (Al), β, and (Si). The addition of Cu to 6061 produces more equilibrium phases. Low levels of Cu in 6061 will form the equilibrium phases of (Al), Q, β, and (Si), while higher Cu content produces (Al), Q, $CuAl_2$ (θ), and β (Figure 1). The Q phase is a hexagonal quaternary phase containing Al, Si, Mg,

and Cu [6]. X-ray diffraction (XRD) of hot rolled 6061-T651 alloy shows the presence of (Al), β, Mg_5Si_6, Al_7Cu_2Fe, and (Al, Fe, Si) phases [7].

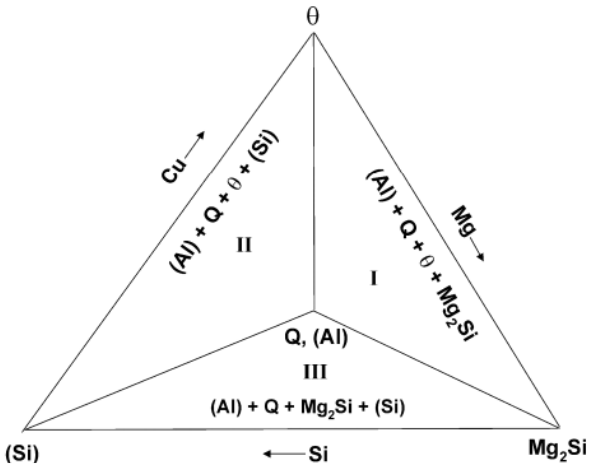

Figure 1: Quaternary equilibrium phase diagram for Al-Si, Mg, and Cu. The line coming down from the θ corner represents the composition where Si and Mg are at a 1:1 ratio. In alloys with low Si content, equilibrium phases are in quadrant I. When there is low Mg, quadrant II phases are present, and when there is low Cu, quadrant III phases are present. [6].

1.2.1 T6 Heat Treatment

The T6 heat treatment allows heat treatable alloys, like 6061, to precipitate and increase the strength of the alloy by impeding dislocation motion. The steps involved with this heat treatment are: solutionizing the alloy, quenching the alloy, then artificially aging it to peak hardness. Solutionizing is required to dissolve alloying elements into a solid solution of (Al), the precursor for precipitation. The alloy is heated to a temperature high enough to change the thermodynamics of the system to dissolve alloyed elements into a solid solution after a period of time needed for diffusion. As the alloy is cooled, thermodynamics will favor uncontrollable precipitation. To stop the kinetics of this reaction, the metal is quenched, forming a metastable supersaturated solid solution. After quenching, the alloy is reheated to a lower temperature for a period of time to control the type and amount of precipitation that occurs. Controlling the aging temperature will optimize the properties of the 6061 alloy. 6061 is solutionized at 530°C and heat treated at 170°C for 8 hours [8]. The progress of precipitation, starting from the solid solution, follows the sequence of forming Guinier Preston (GP) zones → β'' → β' → β [6]. Precipitates start as coherent precipitates that have the same structure as the matrix, but strain the lattice due to a difference in bond lengths. Incoherent precipitates have their own separate structure and boundary from the matrix. The strength from the heat treated alloy comes from the coherent needle shaped monoclinic β'' precipitate that form along the <100> family of directions [6]. The Cu also forms an intermediate lath L phase, a precursor to Q' and Q, that also increases the strength of 6061-T6.

1.2.2 Extrusion

Extrusion is a forming process that utilizes a ram to force a billet of material through a die. This process is usually done with ductile metals (Figure 2). The billet plastically deforms and conforms to the shape of the die as it exits the back end. This process typically forms elongated grains in the metal, which produce favorable properties in the extruded direction [9]. Material at the surface will move slower and exhibit higher levels of deformation than material in the

middle of the die. Extrusions can be done hot or cold, but hot extrusions are more common and increase the ductility of the billet [10]. Hot extrusions occur above the recrystallization temperature and would recrystallize any cast or cold worked microstructure, mitigating strain hardening. Precipitates can also dissolve in the alloy prior to being forced through the die. The high temperature increases the material's ductility, allowing the die to produce a greater percentage of reduction and conformation to the final product shape. The disadvantages of hot extrusions are the same as the advantages of cold extrusions. During hot extrusion, oxides tend form on the surface of the material. The oxidized material requires more force to be pushed through the die. This will shorten the life of the die as it produces a faster rate of die wear. Hot extrusions also negatively affect the surface finish of the extrusion and decrease the tolerance of the final product [9].

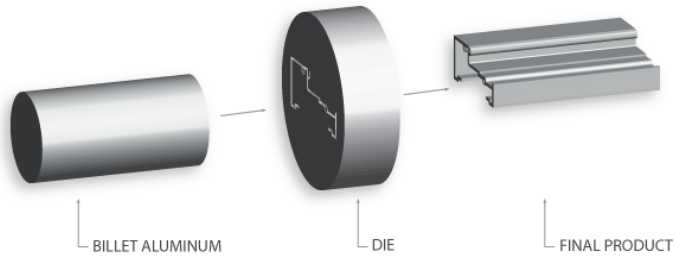

Figure 2: Schematic of the aluminum extrusion process. An aluminum billet is forced through a die and takes the shape of the profile cut into the die [11].

Extrusions can also be direct or indirect. Direct extrusions push the billet through a die on the opposite end of the ram. Indirect extrusions have the die fixed on the end of the ram. As the ram pushes forward, the extrusion is formed in the opposite direction behind the ram. Direct extrusions have higher amounts of friction and require more force, but indirect extrusions are more complicated and delicate, limiting the amount of force that can be applied during processing [9].

Cast billets of 6061 have the following three phases at elevated temperatures. At 587°C, liquid (L)↔ Al + Mg_2Si; at 578°C, L ↔ Al + β(AlFeSi) + Si; and at 550°C, L ↔ α-Al(FeMn)Si + Mg_2Si + Si + Al [12]. The precipitates from the first two reactions, Mg_2Si and β(AlFeSi), are strong and brittle. They can cause frictional tearing and incipient melting when extruded [13]. To prevent tearing and incipient melting, the billet is homogenized. This forms a fine dispersion of Mg_2Si that will dissolve when hot extruded and transforms the β(AlFeSi) →α-Al(FeMn)Si. The temperature of the extruded billet depends on the extrusion speed, the shape of the die and the initial temperature of the billet. The lower temperature limit for 6061 extrusions is the solvus temperature, 529°C, where extrusion speeds can increase. The upper limit to the extrusion speed is determined by the temperature as billet reaches the die. This temperature is increased due to the metal's deformation and frictional heating [12]. If the critical temperature is exceeded, tearing and melting can occur.

1.3 Fatigue

Ninety percent of all failures in mechanical devices are due to fatigue [14]. Fatigue is the cyclic loading of a material that causes failure due to the presence of the following three conditions: a tensile stress below the yield strength of the material, variations in applied stresses, and a large number of cycles [14]. Two variables in fatigue are the mean stress, σ_m, and the stress amplitude, σ_a (Figure 3).

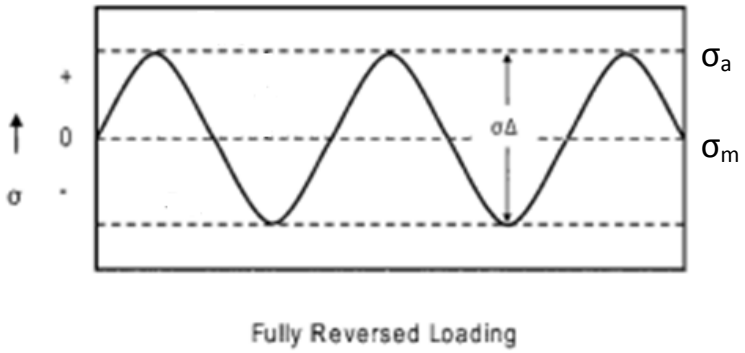

Figure 3: Cyclic loading stress of fully reversed loading [14]. Mean stress is zero, and the stress amplitude is equal and opposite in tension and compression.

Increasing mean stress will lower the fatigue strength. The mean stress and stress amplitude for a given number of cycles can be modeled with the Gerber curve for ductile metals. The Goodman line is a more conservative estimate especially with data that has a high degree of scatter. If the design parameters use the yield strength rather than the ultimate strength, then the Soderberg line can be used (Figure 4) [14].

Figure 4: As mean stress increases the stress amplitude must decreases. The Gerber and Goodman lines use the material's ultimate strength, σ_u, and Soderberg uses the yield strength, σ_y, to find the balance of mean stress and stress amplitude [14].

Below is the Soderberg equation relating stress amplitude to mean stress (Eq. 1). σ_m is the mean stress, σ_y is the yield strength, σ_e is the fatigue strength of N number of cycles at zero mean stress, and σ_a is the fatigue strength of a material after N number of cycles with the

applied mean stress [14]. In the fully reversed loading condition, the mean stress is zero and the equation becomes simplified.

$$\sigma_a = \sigma_e \left(1 - \left(\frac{\sigma_m}{\sigma_y}\right)\right) \quad \text{Eq. 1}$$

Generally, metals with high tensile strength will also have high fatigue strength. During the initial cycles of fatigue, metals that were heat treated to increase hardness undergo cyclic softening while soft metals undergo cyclic hardening as dislocations are either increased or decreased [7]. Based on how long it takes for failure to occur, fatigue falls into two categories: low cycle and high cycle. Low cycle fatigue occurs when the stress is high enough to produce plastic deformation. This forms a hysteresis loop in the stress-strain diagram and causes the metal to fail under a low number of cycles. In high cycle fatigue, the number of cycles range from 10^6 to 10^8. The applied stress is low enough to keep the strain in the elastic region. Lowering the applied stress will increase the number of cycles until failure occurs. Although the metal is undergoing elastic deformation at low stresses, plastic deformation can be present at cracks where there are stress concentrations or along slip planes and initiate cracks [14].

Fatigue occurs through crack initiation, crack propagation, and fracture (Figure 5). During initiation, slip bands shear at 45 degrees to the applied tensile force, where the shear stress is greatest. The continual shearing of these planes will build up and start small cracks. Once they reach a critical size, they will act as stress risers and begin to grow perpendicular to the force, resulting in crack propagation. Every cycle of minimum to maximum stress will form striations as the crack grows with each cycle until the stress is too high for the reduced cross sectional area that remains [14]. The high stress will then cause failure. Individual striations are not visible by eye, but can be seen in larger groups known as “beach” marks [10].

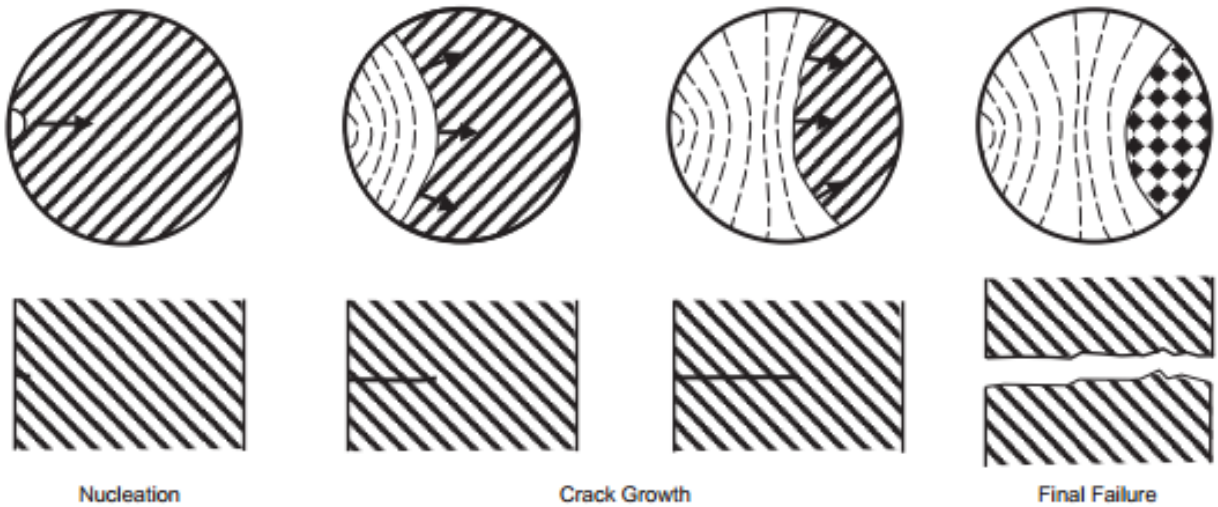

Figure 5: This schematic shows the steps of fatigue and how a crack propagates across the cross sectional area. Beach marks can be seen as the crack grows with each cycle until the final area fails under the applied stress.

Some metals, like steels, have an endurance limit at 35-60% of the tensile strength and theoretically will never fail when they are loaded below that stress. Other metals, like aluminum, continuously lose fatigue strength as the number cycles are increased (Figure 6).

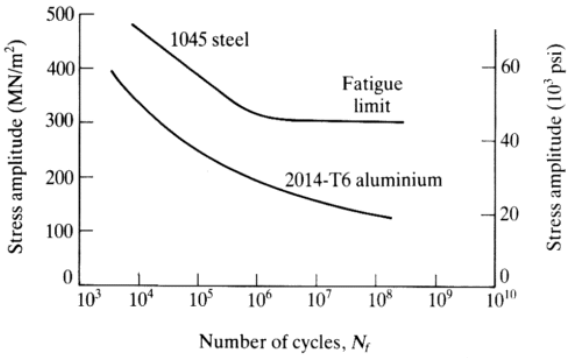

Figure 6: Typical S-N curve of steel and aluminum. This shows the fatigue limit of steel and relative fatigue strengths of both materials [15].

Inclusions, surface roughness, residual stresses, and the environment can affect the fatigue strength of a component [10]. Stress concentrations, such as notches or cracks, replace the need for crack initiation through slip, and reduce the fatigue strength. Surface roughness also acts as stress risers for fatigue; the rougher the surface, the lower the life. If the surfaces are hardened, through processes like carburization or nitriding, or if there is a residual compressive stress on the surface, the fatigue strength will increase. Fatigue that takes place in a corrosive environment causes corrosion fatigue and lowers the fatigue strength [10].

1.3.1 Rotating Bending Fatigue Testing

Fatigue tests can be categorized by the R value. The R value is the ratio of minimum stress to maximum stress [14]. Two types of fatigue testing are direct axial loading and rotating beam loading. In axial loading, the entire sample cross-section is under the same stress, which oscillates between maximum and minimum stress. It is able to achieve many values for the R ratio, and can be either strain controlled or stress controlled. Strain controlled testing limits the amount of plastic deformation and more closely replicates real life situations where the motion of usable parts are constrained [16]. Rotating bending fatigue (RBF) is tested using a fully reversed R.R. Moore fatigue machine, and is stress controlled based on the applied load at the end of the beam. The maximum stress in tension is equal to the maximum stress in compression, and correlates to an R value of -1 (Figure 7). At any instant in time, the sample reflects a beam in bending where the top surface is under maximum tension and the bottom surface is under maximum compression [10]. Crack initiation will occur on the surface where there is a maximum stress. This is due to the uneven stress distribution of a beam in bending. RBF can be run at high speeds without affecting the fatigue results below 200 Hz [17].

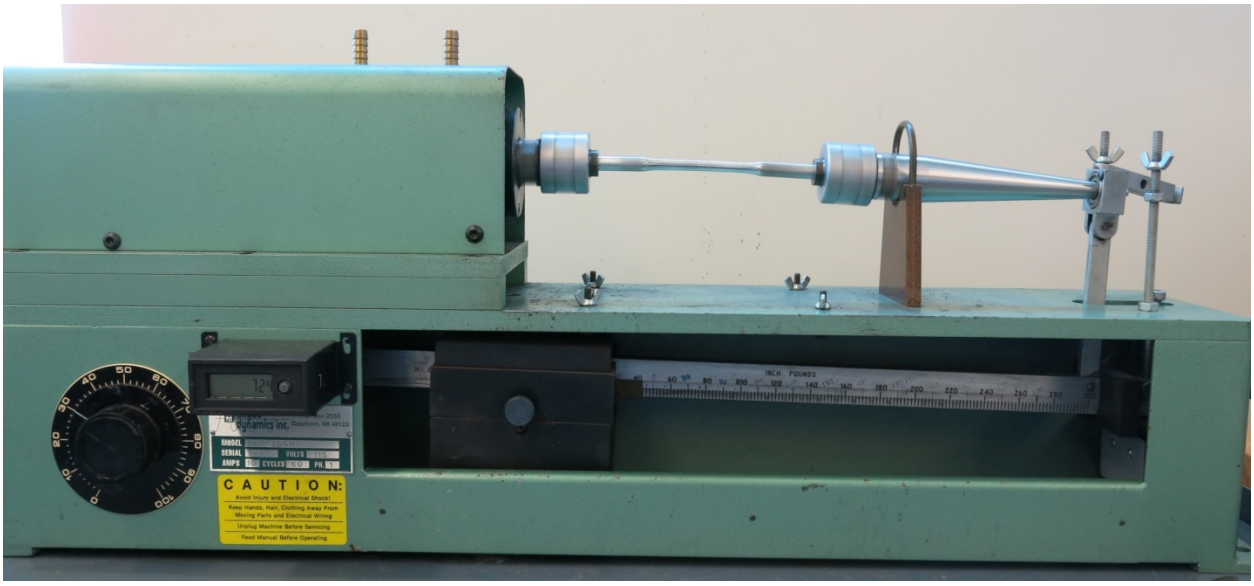

Figure 7: RBF 300 rotating bending fatigue machine. The sample, loaded with a moment, is a beam in bending with r = -1.

1.3.2 Fatigue Statistics

Fatigue data is plotted as an S-N curve on a graph with stress amplitude on the y-axis (S) and the log of the number of cycles until failure on the x-axis (N). High cycle fatigue shows a greater variability in this data than low cycle fatigue [18]. Increased variability means that more samples need to be tested to produce reliable conclusions. It is impossible to test all of the samples in a population, so a smaller selected sample size needs to be tested to make assumptions about the population. An ideal sample size is over fifty, but often smaller numbers are tested. Most of the time, these samples need to be cut out of the actual structure that will be in use. Statistical data retrieved from fatigue tests include the arithmetic mean (μ), geometric mean, median, and standard deviation (σ). The standard deviation is important because it shows the dispersion of the data. The coefficient of variation (COV) can help in determining the uncertainty of data, and is the standard deviation divided by the mean. In fatigue, the COV can be 0.6 or higher [19].

Fatigue can follow many probability density functions (PDF) like the normal or Weibull distribution (Figures 8). PDFs show the probability of failure at a certain number of cycles (Eq. 2). The normal distribution is best suited for low to medium fatigue strength. The disadvantage of the normal distribution is that the x-axis, number of cycles, starts at negative infinity rather than zero. Weibull analysis is useful because only a small number of samples are needed for failure analysis, and it better fits high cycle fatigue data [20]. It was originally designed for use with failure analysis in fatigue. Weibull analysis is preferred when predicting high cycle fatigue. It is also favored because there is a minimum safe life (N_0) where the reliability is 100% [18].

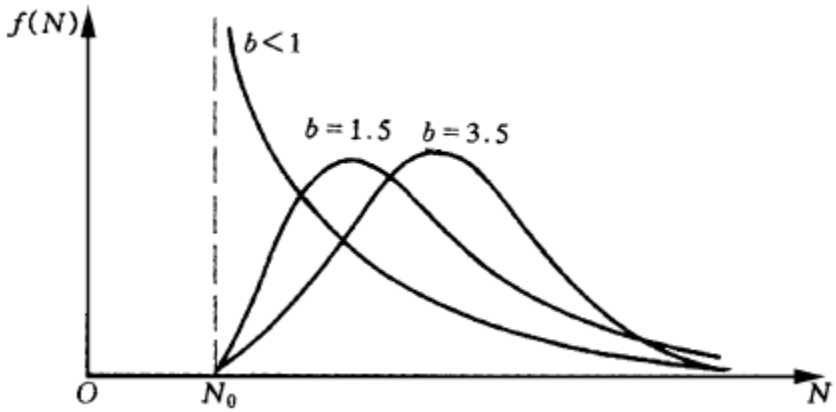

Figure 8: The Weibull probability density function based on the parameters of β and α, Eq. 2. At β= 3.57 the curve is normal, and at 1 the curve is exponential [18].

$$f(x) = \frac{\beta}{\alpha}\left(\frac{x}{\alpha}\right)^{\beta-1} e^{-\left(\frac{x}{\alpha}\right)^{\beta}} \qquad \text{Eq. 2}$$

The α parameter is the characteristic life, where 63.2% of the parts fail. β is the slope parameter and describes the shape of the curve. The standard deviation increases with an increase in α and decrease in β. Failure modes can be predicted with the β value. When β < 1, failure is indicative of defects due to the manufacturing process. β = 1 shows a distribution of random failures, and β > 1 accompanies wear out failures. One minus the derivative of the probability distribution function produces the cumulative distribution function. This shows the percentage of failures after a certain life, x.

1.4 Welding

Welding is a process that joins two or more materials into a single part. Most welding processes involve melting the parts together with a filler material. Tungsten inert gas (TIG) and metal inert gas (MIG) are examples of processes that involve melting metal to join work pieces together. The finished work piece has three different zones on both sides of the weld joint: the weld nugget, the heat affected zone (HAZ) and the base metal (BM). The weld nugget can also be called the fusion zone where the work piece melts together and forms a dendritic structure. The nugget experiences the most heat intensity during welding, causing the greatest loss of material properties. The HAZ is the area around the weld nugget that has not been melted but has its microstructure and properties changed from the diffusion of heat. The rest of the work piece is made of the base metal that has not gone through any changes from the welding process. Because of the high heat intensity and changes in microstructure, the weld nugget and the HAZ have lower mechanical properties compared to the base metal. One way to reduce the change in properties is to use less heat and not melt the metals to join them.

1.4.1 Friction Stir Welding

Weld processes that do not melt metals to join two parts together are called solid state joining processes. These processes use vibrations, explosions, or frictional heat to join different work

pieces together. Friction stir welding (FSW) is a solid state joining process that uses plastic deformation and frictional heat to join metals [21]. The process involves holding the work pieces butted together against a backing plate and welding it with a tool similar to a mill bit. A rotating pin tool pushes into the seam against the backing plate and travels along the joint while rotating, "mixing" the metals together. The welding tools can have many designs, but they all include a scrolled shoulder that keeps the material inside the joint and a pin with different geometries, flutes, and thread counts, that penetrate the joint and weld the material. Due to the lower temperatures compared to fusion welding, the metals do not melt but still form the same zones as traditional welds (nugget, HAZ, and BM) along with the thermo-mechanically affected zone (TMAZ) between the nugget and the HAZ (Figure 9). FSW has multiple advantages compared to fusion welding techniques such as limited voids or cracking in the weld, smaller distortion of the work piece, and no need for filler metal [22].

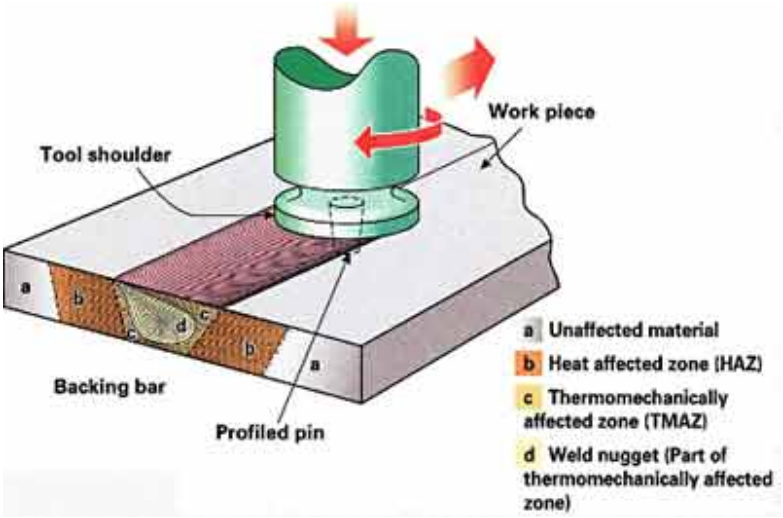

Figure 9: Friction stir welding process with different zones identified after the pin has joined the metals [23].

Residual stresses are present in the weld zone due to the frictional heating and deformation. If these residual stresses are tensile, they can severely lower the fatigue strength of the metal. The stresses in the weld can be in any direction, and experiments have been done to find ways to reduce the tensile stresses and increase the compressive stresses in the material. Cooling has been used in 2xxx series aluminums to decrease the residual stresses, but it was only able to lower the stresses in the stir zone [24]. Another method used was to put the material in tension as it is being welded. After the welding is complete and the load is released, the material will relax and induce a compressive stress. The lower heat distortion of FSW results in reduced residual stresses, making deformation control during welding easier compared to fusion welding [25].

FSW welds are not symmetrical. They have an advancing side and a retreating side due to the relative rotation of the pin during welding. The side where the pin rotation is in the same direction as the tool travel is considered the advancing side. The side that has opposing tool rotation to travel direction is the retreating side. The properties of either side are not the same due to the material flow around the pin when welding. There is a combination of shearing,

extruding, and forging that occurs. The advancing side picks up material from the front of the weld. As the tool moves forward and this material gets caught in the rotation of the pin for a few rotations before it gets deposited on the back of the retreating side. The deposited material gets "forged" together in the joint as new material continues to be forcefully deposited on previous layers. As this material circles, it is also pushed down along the pin until it reaches the bottom of the part where it is pushed out and up. The material undergoes a large amount of strain and is highly deformed. The material on the retreating side gets squeezed, like an extrusion, between the pin and the plate [26].

1.4.2 Friction Stir Welding vs. Fusion Welding

Friction stir welded metals have favorable mechanical properties compared to fusion welded metals since the metals being joined do not melt (Figures 10 and 11). There is less distortion in the part, lower porosity, lower residual stresses, no compositional changes when comparing the nugget and the HAZ, no hot cracking, and less grain growth [27]. FSW is used over fusion welding because it can weld metals together that are normally not weldable, like dissimilar metals and high strength aluminums. These expanded applications result from lower heat input and stirring rather than melting. The superior properties and can be attributed to the different microstructural changes that FSW causes in a joint. A FSW 6063-T6 aluminum stir zone microstructure contains fine equiaxed grains while its TIG welded counterpart contains dendritic structures (Figure 12). The fine equiaxed grains found in the FSW weld nugget form due to dynamic recrystallization that occurs during the FSW process [22]. Dynamic recrystallization is the process where recrystallization occurs during deformation, where the strain rate is high. The material in the weld joint is subject to high strain rates and high temperatures to drive fine grain recrystallization. This occurs in metals that twin and have low stacking fault energy. Aluminum has high stacking fault energy and allows dislocations to move easily [7], but FSW of aluminum is an exception to this rule. This allows metal that has undergone FSW to regain some strength from the fine grains it produces. The dendritic microstructure found in the weld nugget of TIG welded metal forms from the fast heating of base metal and fast cooling of the molten metal [22]. The dendritic structure is not as strong as fine equiaxed grains because dendrites do not impede dislocations as well as fine grain structures. FSW are also different from fusion weld because they have the TMAZ region which has induced strain due to the friction of the shoulders. This occurs at the boundary next to the stir zone where material gets sheared from the front of the tool and rotated in the stir zone. The grains in the TMAZ are distorted and can undergo recrystallization, although they may not be equiaxed [28].

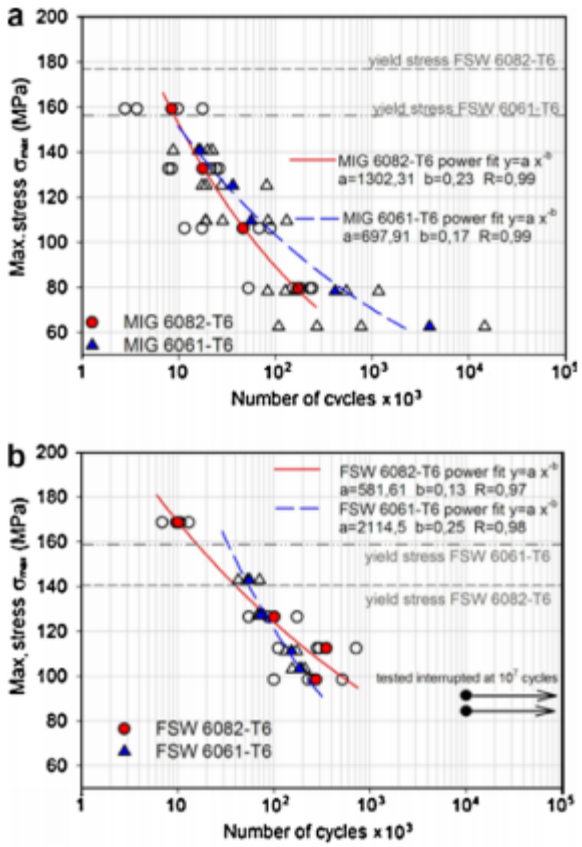

Figure 10: Comparison of low and medium cycle fatigue strengths of a) FSW and b) MIG welded 6061 aluminum [29]. At 10^5 cycles the FSW fatigue strength is 125 MPa while the MIG fatigue strength is 110 MPa.

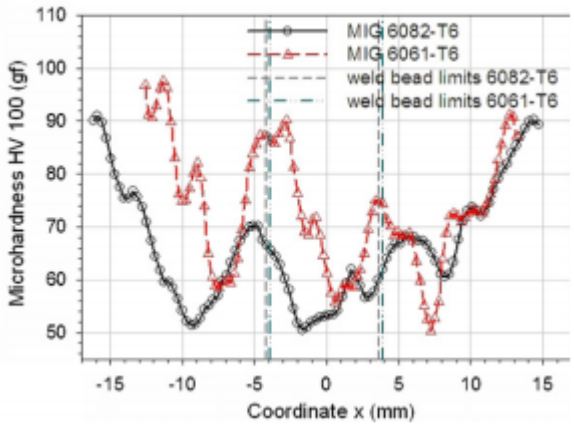

Figure 11: Microhardness of MIG welded 6061 and 6082. This can be compared to Vickers hardness of FSW 6061 as part of this report and in later Figure 16 [29]. The hardness of FSW welds are about 10 HV greater than MIG welds.

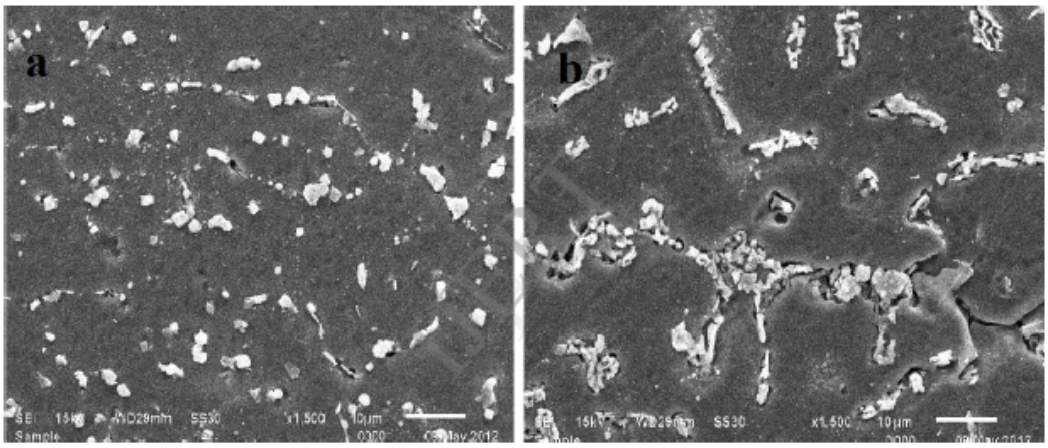

Figure 12: Microstructure of weld nugget in a) FSW and b) TIG weld [30]. The TEM micrograph show the smaller grain size that is present in the dynamic recrystallized nugget of the FSW compared to the dendritic nugget of the TIG weld.

1.4.3 Bobbin Tool Friction Stir Welding

FSW can be done with many different tools and one such tool that is used is the bobbin tool. The bobbin tool has a shoulder on the top and the bottom of the pin, and is pushed into the side of the part (run in) before a steady state weld is achieved. At the end of the weld (run out) the pin exits the opposite side of the part. This last bit is not a steady state process and is removed from the final product. The bobbin tool does not require a backing plate because there is a shoulder for both the top and bottom of the work piece (Figure 13). The force that is traditionally held by the backing plate is now held between the top and bottom shoulders. This produces greater tool wear, but has other advantages. There is no weld root in the joint since the tool penetrates the full depth of the weld. This eliminates the possibility of having a stress riser due to a crevice on the bottom of the weld [25]. Frictional heat is also provided by the top and the bottom shoulders that offer a uniform heat input that makes the weld more symmetrical [31].

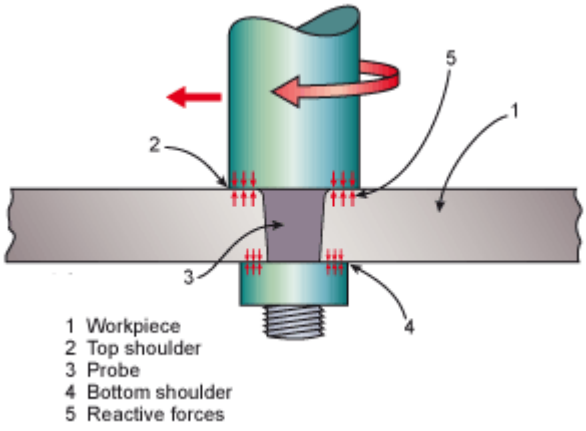

Figure 13: FSW with bobbin tool [31].

The second shoulder at the bottom results in an hourglass-shaped weld unlike a conventional FSW where the weld would have a more triangular shape (Figure 14). This hourglass morphology will give symmetry to the weld so that it has similar properties at the top and bottom of the work piece. This symmetry is evident in hardness tests, where the hardness values of a weld made with a bobbin tool and conventional tools are compared (Figure 15). The bobbin tool weld has more uniform hardness throughout the whole weld while the conventional weld's hardness narrows as it reaches the bottom of the work piece. Unfortunately the bobbin tool is not as optimized as the conventional FSW tool, and has more porosity in the weld joint.

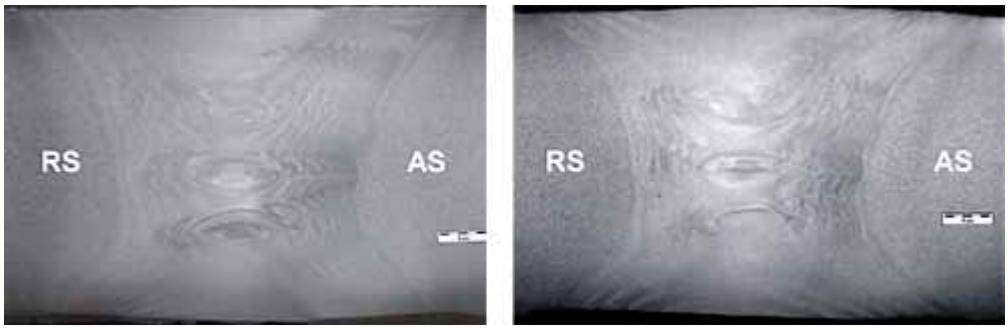

Figure 14: Cross section of the hourglass-shape in 6082 aluminum FSW with bobbin tool [31]. RS is the retreating side and AS is the advancing side.

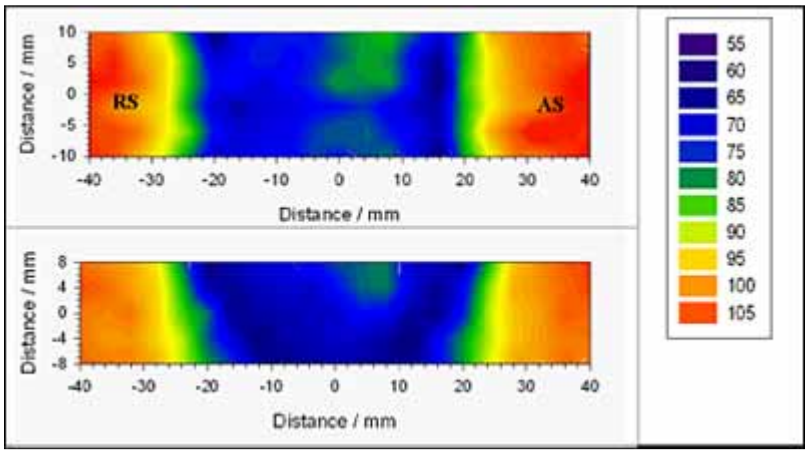

Figure 15: Hardness values of FSW 6082 aluminum: bobbin tool (top) and conventional tool (bottom) [31]. The conical shape can be seen in the conventional tool due to a non-uniform heat distribution.

1.4.4 Friction Stir Welding of 6061

As discussed in section 1.2.1, the high strength attributed to 6061-T6 aluminum results from the elements Mg and Si forming the β" precipitate Mg_5Si_6, 4 x 4 x 50 nanometers in size. These precipitates are stable at temperatures below 200°C. During FSW the precipitates are dissolved because the temperatures are between 200-250°C [22]. Even though the aluminum loses its strengthening precipitates, the weld zone retains some strength from the formation of fine, equiaxed grains, smaller than those of the base metal along with solid solution strengthening. The small recrystallized grains form due to dynamic recrystallization in the presence of high

strain during deformation. There is also evidence under TEM that the nugget contained other coarse dispersoids in the grains and along the grain boundaries containing Al, Cr, Mn, Fe, and Si [7]. In the HAZ, there is dissolution and coarsening of precipitates [7]. Where temperatures reach up to 200^{o}C at the HAZ, there is dissolution and a low precipitation of β', Mg_2Si, particles that have less strengthening properties compared to β" resulting in a lower hardness [22]. The hardness of FSW 6061 begins to lower at the HAZ and through the TMAZ, but recovers some strength at the weld nugget (Figure 16). The low hardness zone is in the HAZ at the border of the TMAZ [7]. This is where most of the failures occur during fatigue and tensile testing.

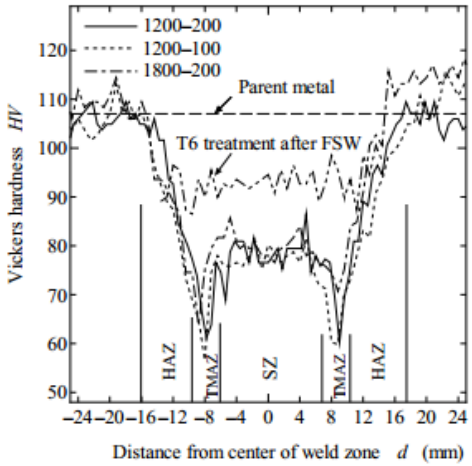

Figure 16: Microhardness of FSW 6061 aluminum [32]. The different hardness profiles are produced from varying welding parameters.

Welding speed and rotational speed also affect the microstructure of the FSW. As the weld speed decreases, there is a growth in the width of the low hardness zone and a drop in the hardness **[7]**. Rotational speed has little effect on tensile strength but a change in weld speed caused a 5.3% change in the tensile strength of the aluminum (Table V). The S-N curve for FSW 6061 shows that the FSW has lower fatigue strength compared to the parent metal, especially in the high stress region. Also, the stress level effects the location of the fracture. Fracture occurs at TMAZ under higher stress levels, while fracture occurs at HAZ under lower stress levels (Figure 17).

Table III: Tensile Strength and Elongation Comparison of Parent Metal and FSW 6061 Aluminum, with Varying Weld Parameters [32]

Designation	Tensile strength, σ_B (MPa)	Elongation, δ (%)
Parent metal	308	15
1200-100	194	7
1200-200	205	7
1800-200	204	7

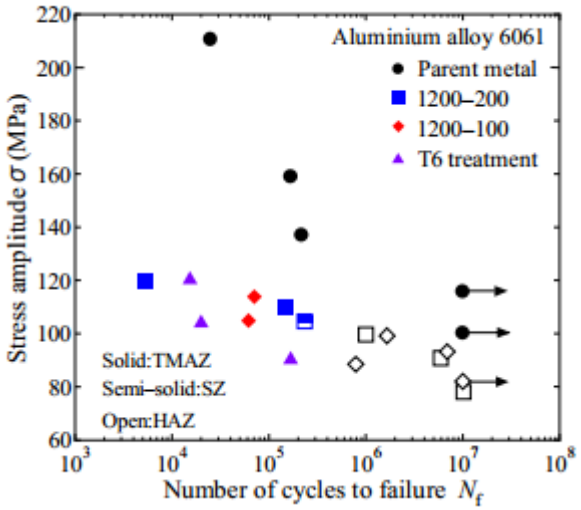

Figure 17: S-N curve of FSW 6061, R= -1 fully reversed loading [32]. Different weld parameters are compared for FSW. At 10^5 and 10^6 cycles the fatigue strength of FSW is 115 MPa and 100 MPa respectively. The base metal fatigue strengths at those cycles are 160 MPa and 120 MPa respectively.

2 Problem Statement

Sapa Extrusions lacks high cycle fatigue data for FSW 6061-T6 aluminum using the bobbin tool. It is expected that failure will occur between the TMAZ and HAZ where the hardness is lowest. Literature shows that fully reversed fatigue of FSW 6061-T6 has a high cycle stress range of 90-120 MPa. Testing will be done using rotating bending fatigue on machined samples of FSW extruded plate to produce an S-N curve of the data. Fatigue tests of FSW samples will be compared to baseline unwelded 6061-T6 samples. Baseline 6061 has high strength, so ideally the welding process would join the plates while limiting the loss of material properties. Failure distributions of the FSW samples will be analyzed. Also, the fatigue failures will be observed to find the location of failure in the weld. Further analysis will diagnose premature failures and look for reasons why crack initiation occurred.

3 Experimental Procedure

To test the fatigue strength in FSW aluminum, the entire weld zone must be tested and loaded so that the same stress is induced across the weld region. Sapa provided two bobbin tool FSW plates for testing. The plates were first machined into blocks and then turned down into cylindrical samples for fatigue testing. The FSW pin dimensions are a 1:1 ratio of depth to width at 12 mm and the width of the shoulder is at a 2.5:1 ratio with the plate depth, 30 mm (Figure 18). The material started out as 6061-T6 aluminum that was extruded into two 0.5 inch thick plates that were 8 inches wide and friction stir welded down the middle (Figure 19).

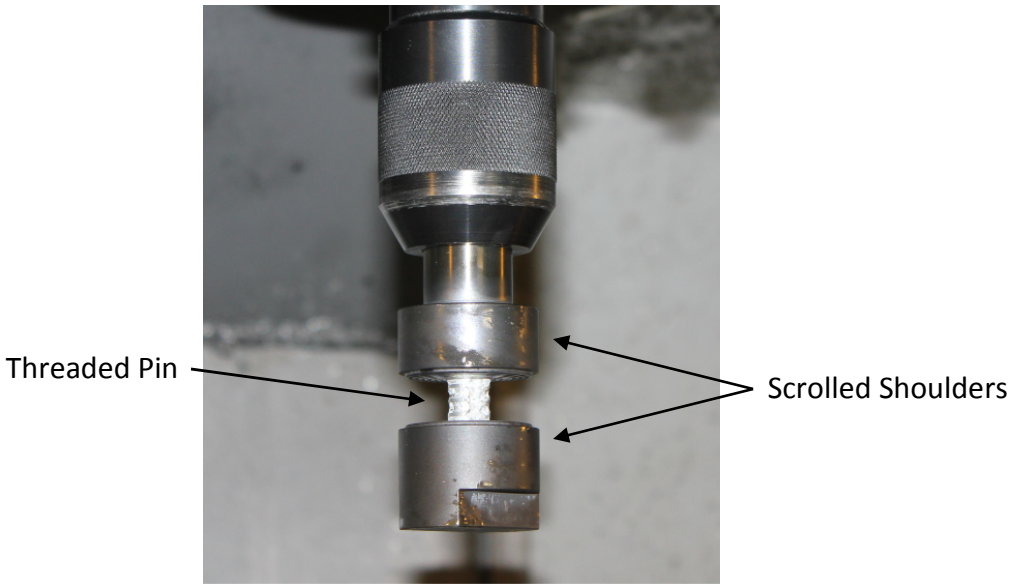

Figure 18: Sapa's bobbin tool for FSW. The pin is 12 mm in diameter and the shoulders are 30 mm in diameter.

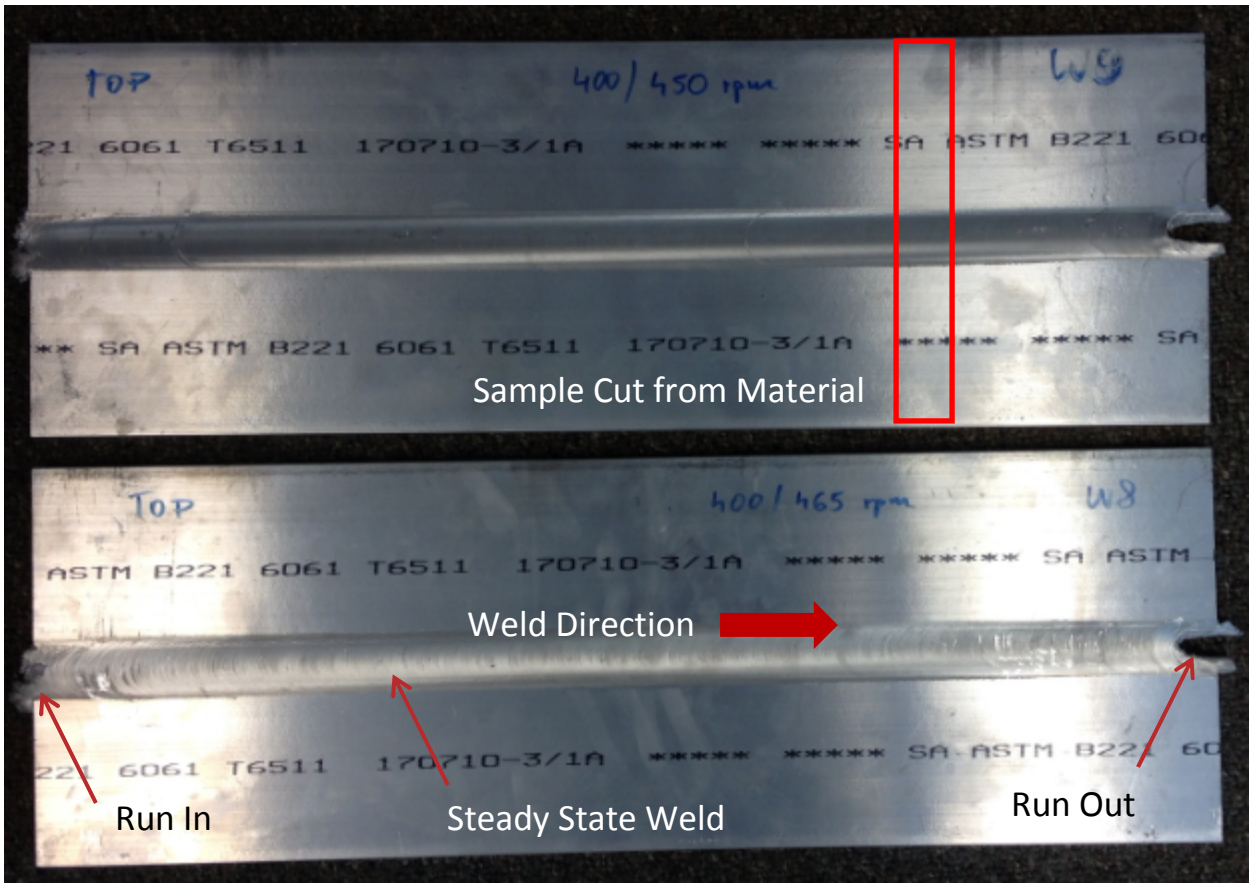

Figure 19: The two plates that were provided by Sapa. They were sent to Cal Poly as pre-cut fatigue samples.

Preliminary testing was conducted on one of the plates to get an idea of the size of the weld zone. Once the weld zone size was known, fatigue samples were designed that would include the entire zone to allow for complete testing.

3.1 Hardness Testing

A four inch cross section of the FSW plate was cut and mounted in acrylic with the stir zone in the middle. The mounted sample was ground and polished flat down to 6 microns on a diamond polishing pad. The sample was loaded into the microhardness tester and three hardness traverses were made, one halfway down in the middle of the plate's thickness and the others an eighth of an inch above and below the mid-plane. The three traverses on the top, middle, and bottom tested the accuracy of the hardness measurements as well as the variability in hardness depending on depth. Each profile included many hardness tests that were taken every 20/1000th of an inch with a Vickers diamond indenter at 300 grams force. The indentations were measured in microns across both diagonals, and translated in to hardness values via a Vickers microhardness conversion table. All three profiles overlaid each other well, and the profile across the weld quantified the extent of the weld zone (Figure 20). Once the cross section hardness leveled out past the HAZ and returned to the base metal extruded hardness, the width of the weld zone was approximated. The hardness of the weld zone is proportional to the strength, and we expect that fatigue failure will occur on the low hardness regions. It was found that the weld zone was about 2 inches in width and that the lowest hardness was about 0.5 inches from the center of the weld on either side of the stir zone. The low hardness is at the edge of the TMAZ where the most aging has occurred and no grains are recrystallized. This profile is similar to the one in literature (Figure 16). The weld sizes are different due to the pin size difference, but the shape and low hardness values are similar.

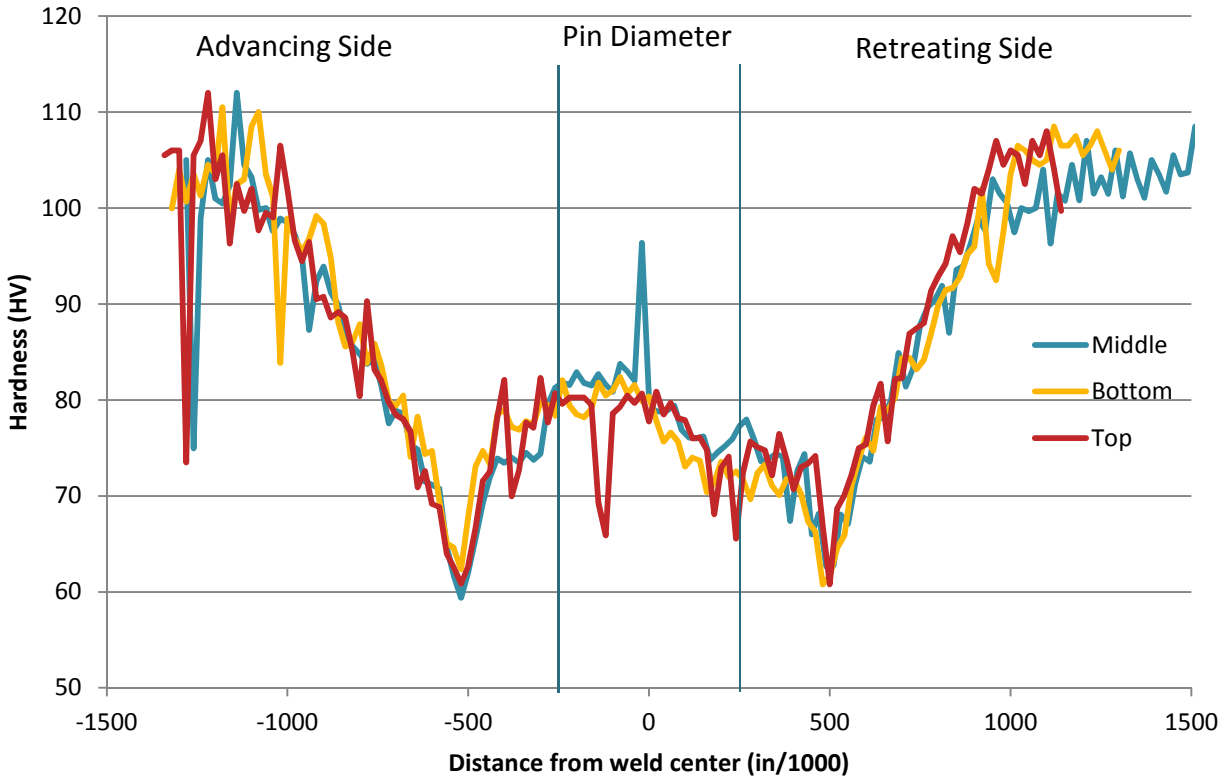

Figure 20: Microhardness of the 6061-T6 plate with 300 gf and 5 second hold time. Comparison between the hardness of the top, bottom, and middle of the weld shows that their hardness is similar. The hardness drops in the HAZ from aging before regaining some strength in the stir zone due to recrystallization.

3.2 Macrostructure

A cross section of the 0.5 inch plate was cut and macro etched with a solution of 65% nitric acid, 32% hydrochloric acid, and 3% hydrofluoric acid (Figure 21). This brought out the grain structure and allowed it to be visible without a microscope. At the surface of the extruded plates, equiaxed grains can be seen. These recrystallized during the process of extrusion. The high strain and deformation that occurs at the surface from the shearing of the material past the die, builds up dislocations, and the added heat used to make the billet more formable is able to recrystallize those grains. Fine equiaxed grains, smaller than the grains of the base metal, can be seen in the stir zone due to dynamic recrystallization during welding. Curved gradients of material are seen stacked up on one another going into the advancing side of the TMAZ as the pin sweeps up the leading material into the rotation of the stir zone. Both sides of the TMAZ show the hourglass effect due to the heat and shear produced by the shoulders. The HAZ shows some larger grains due to the heat input of the welding process that cause grain growth. This macrostructure encompasses the entire weld region and shows that the locations of lowest hardness are between the TMAZ and the HAZ.

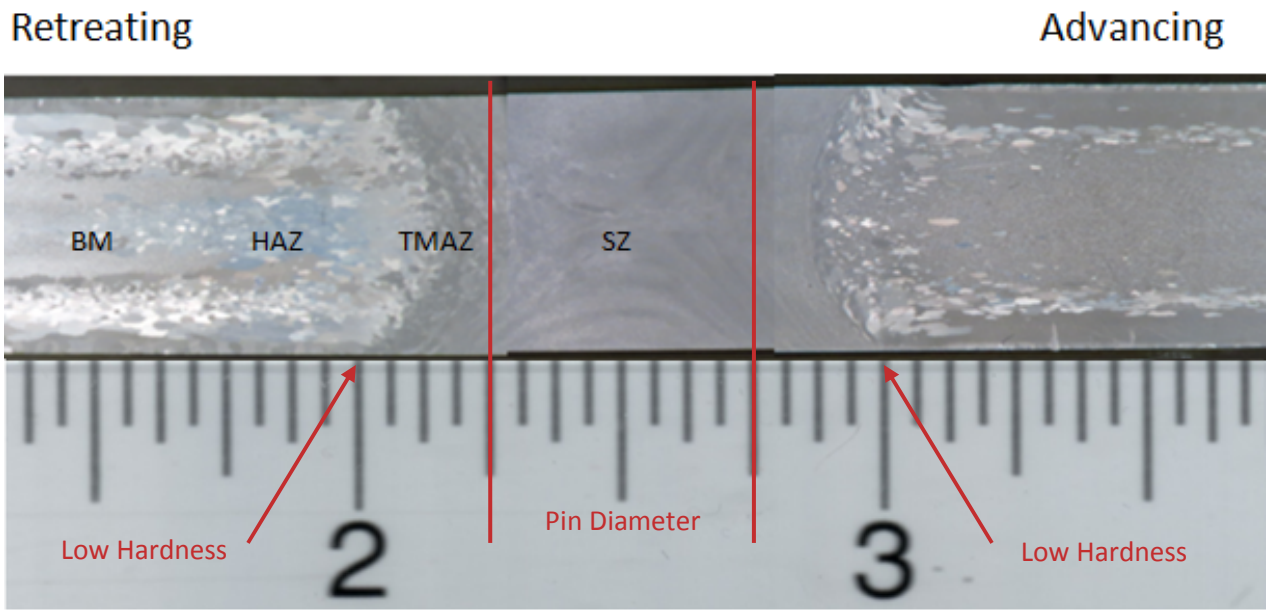

Figure 21: Macroetched 6061-T6 FSW aluminum plate. The pin is 0.5 inches wide and the stir zone is a little larger. The TMAZ has an hourglass shape and beyond that is the HAZ. A thin line of recrystallized grains can be seen at the surface from extrusion.

3.3 Sample Geometry

Standard RBF samples are round and hourglass shaped. This produces a highly concentrated stress in the middle of the sample where failure will occur (Figure 22). From the previous hardness testing, the fatigue samples needed to have a 2 inch reduced section, and the entire region needs to be under the same amount of stress. This will allow the full weld zone to be tested under the same loading conditions, allowing the fatigue test to find the weakest spot in the material rather than the spot that has the highest stress. Also, since the plate thickness is 0.5 inches, the fatigue samples must also be smaller in diameter. The samples were designed to be turned down to a diameter of 10 mm.

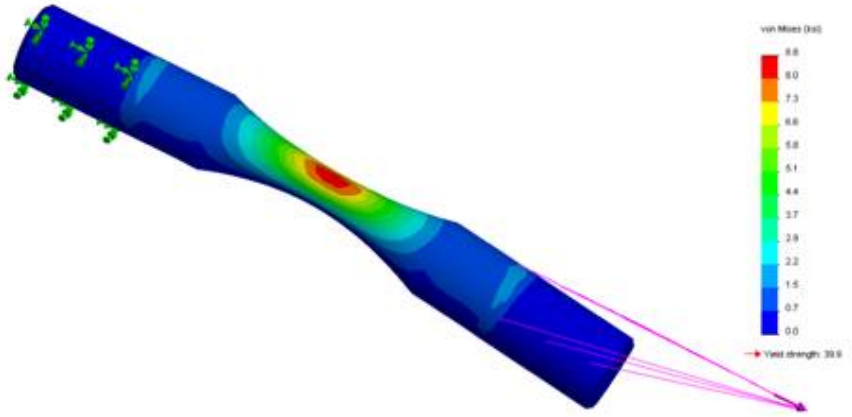

Figure 22: FEA of standard RBF samples. There is a concentrated region of high stress where failure will occur.

A new fatigue sample had to be designed that would fit the functional requirements of size and equal stress. A design for equal stress was found using the bending stress equation and the moment of inertia for a circular cross section.

$$\sigma = \frac{Mc}{I} \qquad I = \frac{\pi r^4}{4} \qquad \text{Eq. 3 and 4}$$

Where σ is stress, M is moment (or force (F) multiplied by distance (d)), c is distance from the neutral axis (which can be redefined as r), I is moment of inertia, and r is cross sectional radius.

Since the diameter of the round bar is 10 mm, the diameter of the reduced section must be smaller. This was specified to be 7.5 mm at the largest end. The applied moment will cause the reduced section farthest from the load to experience greater stress. This end was set to have the radius of 3.75 mm, and a taper would reduce the radius down the reduced section following Eq. 5.

$$r = \sqrt[3]{\frac{4Fd}{\pi\sigma}} \qquad \text{Eq. 5}$$

When equations 3 and 4 are combined, the only variables are F, d, and r. F will be fixed for each test and d will be fixed since the reduced section is always in the same location and the same distance from the applied load. Since F and σ are related, the ratio of F/σ had to be calculated. To do so, r was set at 3.75 mm and σ ranged from 80 to 120 MPa. This provided the ratio used in Eq. 5 to find the curve needed to maintain equal stress. Changing the stress did not change the ratio either. The F/σ ratio was the same up to four significant figures when stress ranged from 80 to 120 MPa. The final equation was only dependent on the distance from the force to provide the needed cross sectional radius. This equation was used in SolidWorks to fit a line to

the third degree polynomial when d ranged from 9.5 to 11.5 inches (Figure 23). These distances were converted into metric unit for the analysis of the equation.

The first design did not meet the requirements of equal stress, as it was modeled with the load being applied at the end of the sample rather than at the end of the gripping arm. The sample had a steeper taper with a thinner section on the side where force is applied. This caused a concentration of higher stress in that region. The fillets going into the grip ends were also too steep and formed stress concentrations during FEA analysis when the mesh was reduced and focused on the fillets. This caused failure to occur at the tail end of the sample next to the fillet (Figure 24). The final design had to simulate the real loading conditions set by the RBF testing machine (Figure 23).

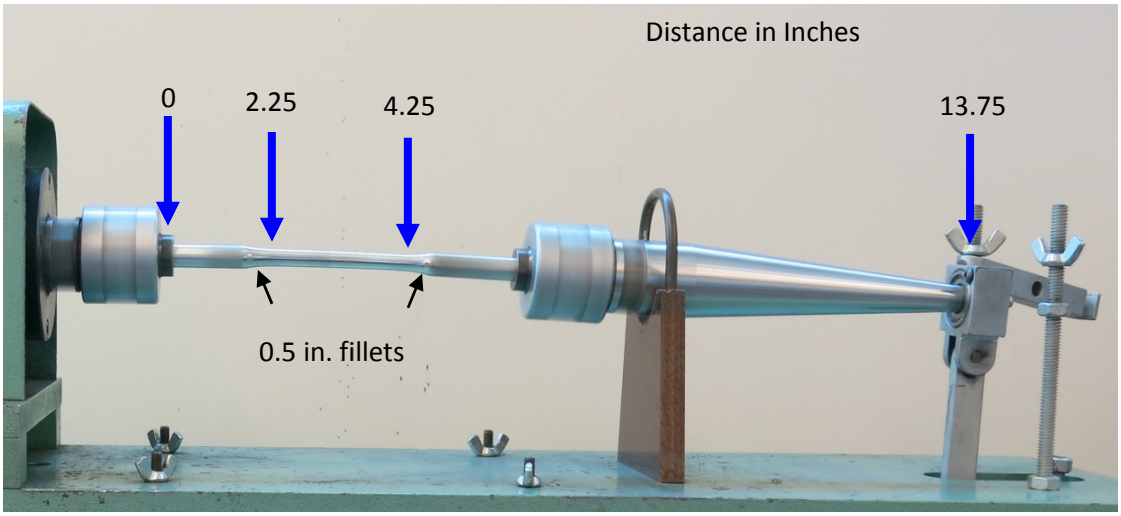

Figure 23: Distances to important regions of the sample while in testing conditions. The distance of where the load is applied is the value that should be used when calculating the moment.

Figure 24: The failure distribution of 5 unwelded base metal samples machined with the initial design show that failure is not random and that there was a design flaw in the model that did not produce constant stress.

To conduct FEA, the sample could not be analyzed on its own. The colleted ends and loading arm needed to be included in the model at the right distances so that the load applied in the FEA will simulate the moment applied by the RBF testing machine (Figure 25). The final sample had a 2 inch reduced section under equal stress, and fillets, 0.5 inches long, in the shape of an ellipse to gradually increase the diameter of the reduced section to 10 mm as it went into the grips. The largest diameter in the reduced section was still 7.5 mm. A new F/σ ratio was calculated and the new Eq. 5 curve was modeled.

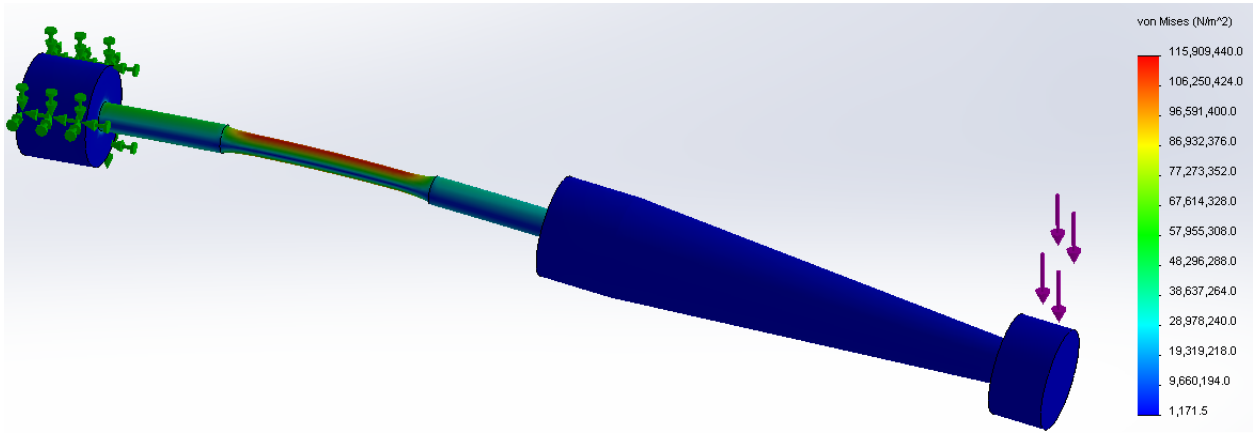

Figure 25: Newly design test sample in actual loading conditions shows that constant stress occurs throughout the reduced section when it is tapered following the correct equation.

This model had a shallower taper in the reduced section and the FEA shows that the sample's reduced section is under the same stress. The model of equal stress was tested again in a practical manner. Five newly designed based metal samples were tested for random failure (Figure 26).

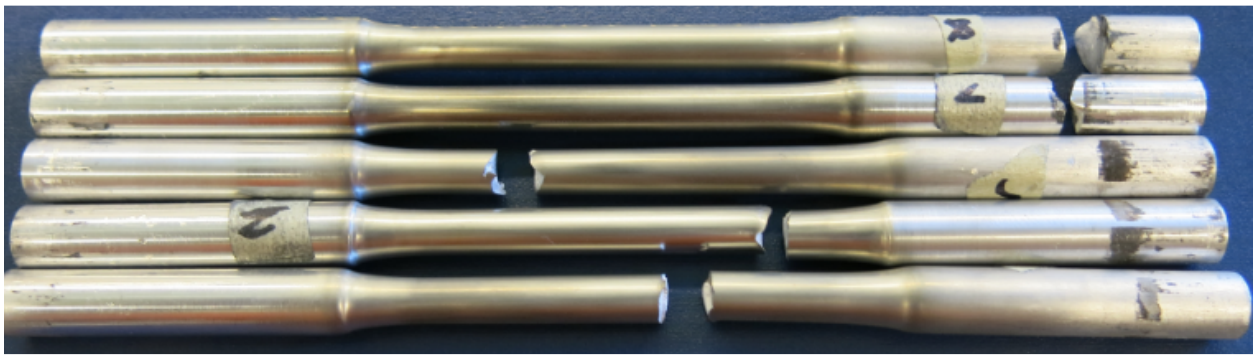

Figure 26: Failure distributions of 5 unwelded base metal samples. The three failures in the reduced section are in different locations and show that the reduced section is under equal stress.

The random failure in the reduced section confirms the model of equal stress, and allows for testing of FSW samples. The two failures in the grips were at the spindle end where the moment is greatest. The reduced area did not make the stress difference between itself and the grip large enough to localize failures in the reduced section. Although this is a problem for the unwelded base metal samples, the FSW samples will not have this problem since the welded metal in the reduced section will be substantially weaker.

3.4 Stain Gauge Testing

Strain gauge tests were conducted for two reasons, first to test the strain at every loading condition so that a stress could be correlated to each moment marking on the loading scale. This stress would be used to produce the S-N curve. The second purpose was to verify that the design did indeed have equal stress across the reduced section. This was done by measuring and comparing the strain at either side of the weld with two different strain gauges (Figure 27). The strain gauge was glued to the surface of the sample. When the sample would bend, the strain gauge would stretch and change its capacitance. The procedure for attaching the strain gauge was to first degrease and roughen the surface with sandpaper. The surface was then cleaned and conditioned with a catalyst to improve bonding. Then the strain gauge was picked up with cellophane tape and glued to the sample. After 30 minutes of curing, the tape was removed at a shallow angle. Once the gauge was bonded to the surface, three wires were soldered to the leads. These leads were wired into the strain indicator P3 unit in a quarter bridge circuit. The box would output units of microstrain as the sample was loaded.

The first strain gauges used were EA-06-120 LZ-120. These smaller gauges were difficult to solder without bridging the terminals. After soldering on the wires to the contacts, the contacts would rip off of the strain gauge. CEA-06-240UZ-12 strain gauges, which are larger, do not have the issue of weak contacts.

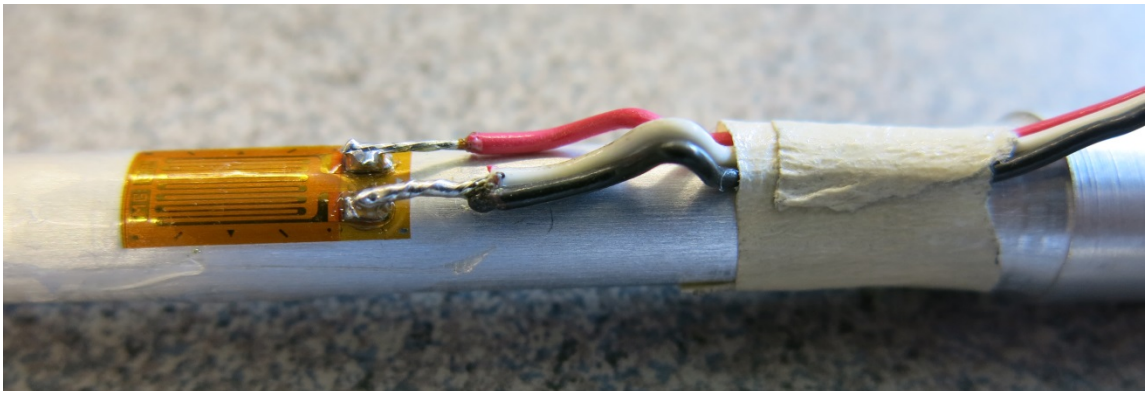

Figure 27: Strain gauge glued to the surface of a sample with soldered leads.

The sample with the strain gauge was fixed into the spindle and the strain was balanced. Then the tail stock was fixed onto the tail end of the sample and loaded with zero moment. The tensile stress would be found by slowly rotating the sample as the strain reached its highest value at the top surface, and the compressive stress was found as the strain reached its lowest value as the gauge was on the bottom of the sample. This was done for every moment used during testing. The two samples that had the strain gauges, one on the middle of the reduced section and the other at the tail end, did not have the same mean stress, and neither had zero mean stress. The stress level for each applied moment was therefore calculated by dividing the stress range by two for both the middle and tail strain gauges, then averaging those values. The strain was converted using the stress-strain equation. Where σ is stress, E is elastic modulus, and ε is strain. The modulus, a material property, of 6061 used in this equation was 69.8 GPa. The stress at the middle and tail end of the samples was concluded (Table IV).

$$\sigma = E\varepsilon \quad \text{Eq. 6}$$

Table IV: Measured Stress from Strain Gauge

Moment	Average Stress (MPa)		Average Stress (MPa)
	Middle	Tail	
Balanced	0	0	0
0	3.4	2.6	3.0
40	112.1	110.8	111.4
42	117.5	116.4	116.9
44	122.7	122.0	122.3
46	128.1	127.6	127.8
48	133.4	131.9	132.7
50	139.2	138.1	138.6

The differences in the stress at the middle and tail end of the sample were not significant to affect the testing condition of equal stress, never exceeding a 1.3 MPa difference. This means that the sample design had constant stress across the reduced section. The stress modeled in the FEA analysis was also compared to the measured stress (Table V). This shows how close the stress in the actual machined samples was to the predicted model.

Table V: Comparison of the Stress Model

		MPa
Applied Moment (in-lbs)	FEA Stress	Actual Stress from Strain Gauge
40	112.1	111.4
50	140.0	138.6

To get the stress in FEA, the force that will be applied by the RBF machine had to be known. Since the RBF machine loads the sample with a moment, the force will be the moment divided by the distance to the area of interest. This area of interest is the point in the reduced section that has the largest radius, where the stress was defined, which was 11.5 inches from the load. The stresses that were predicted by FEA were close to the stresses that were measured with the strain gauges. At the most, there was a 1.4 MPa difference.

3.5 Sample Preparation

The surface finish for fatigue testing is important as small scratches can lower the fatigue strength. This effect is amplified for RBF. The tested samples were polished in the reduced section starting at 600 grit sandpaper to remove all of the machine marks due to the turning process. This was followed by 800 and 1200 grit sandpaper grinding. Each of these steps was done with water lubricant in the direction parallel to the samples' axis, and the surface was cleaned between each step. Finally, the sample was loaded into the RBF machine and polished radially with a 6 micron diamond pad to remove any remaining scratches. This is the best case scenario for testing the fatigue strength of the FSW 6061-T6 material. In most applications of

FSW of extruded plate the surface roughness will be greater than that of the tested samples. The fatigue data, therefore, will also be the best case scenario, meaning that the fatigue strength of parts in everyday use will most likely be lower than that reported.

3.6 Fatigue Testing

Fatigue tests were conducted for 5 baseline samples, 9 FSW samples from the first plate, and 11 more from the second plate. All of the FSW samples from the first plate were tested, while 11 of 30 samples from the second plate were tested. Given more time, more samples could have been tested for a greater number of replications at each stress level. The second plate started out as 50 samples, but 20 of those fell out during machining, probably due to the defects in the weld (Figure 28).

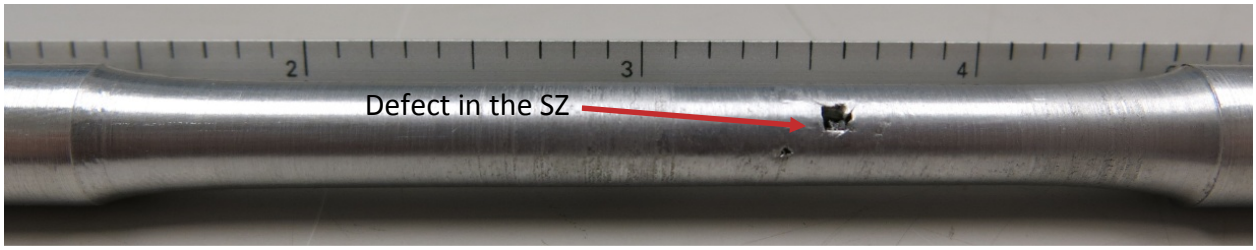

Figure 28: Here is a sample from the second plate that was received after machining. It was not tested since there was a large defect in the surface, but any samples from that plate with similar defects that were not seen on the surface could significantly affect the results of RBF testing.

The polished fatigue samples were loaded into the RBF machine and gripped by the collets on either side. The spindle was turned on with zero load, and once the sample had a smooth rotation between 50-70 Hz, the sample was loaded by sliding the weight to the correct moment. The cycle counter was then started. The shutoff switch was adjusted right above the sensor, so that when the sample broke, or cracked, the machine would shut off and the cycles to failure would be recorded.

There were some areas of concern during testing. Some of these samples did not have smooth rotation, especially in the first batch of material. This could induce a stress loading profile that is not characteristic of the fully reversed loading condition. Also the samples did not have the SZ centered in the reduced section. About 1.5 inches of the retreating side and 0.5 inches of the advancing side were included in the reduced section. This could still allow for failures on either side, as the lowest hardness region of both sides is included in the reduced section, but the increase in diameter past this region on the advancing side will probably limit any possible failures that might have occurring in the HAZ of the advancing side.

4 Results and Analysis

All of the fatigue samples from the first and second FSW plate failed within the reduced section. There were failures on both the advancing and the retreating side, and all but one sample failed in the HAZ or SZ (Figure 29). The majority of the failures occurred on the retreating side, but it is

unknown whether the retreating side was weaker or if the proximity of the advancing side to the edge of the reduced section caused this imbalance of failures (Table VI).

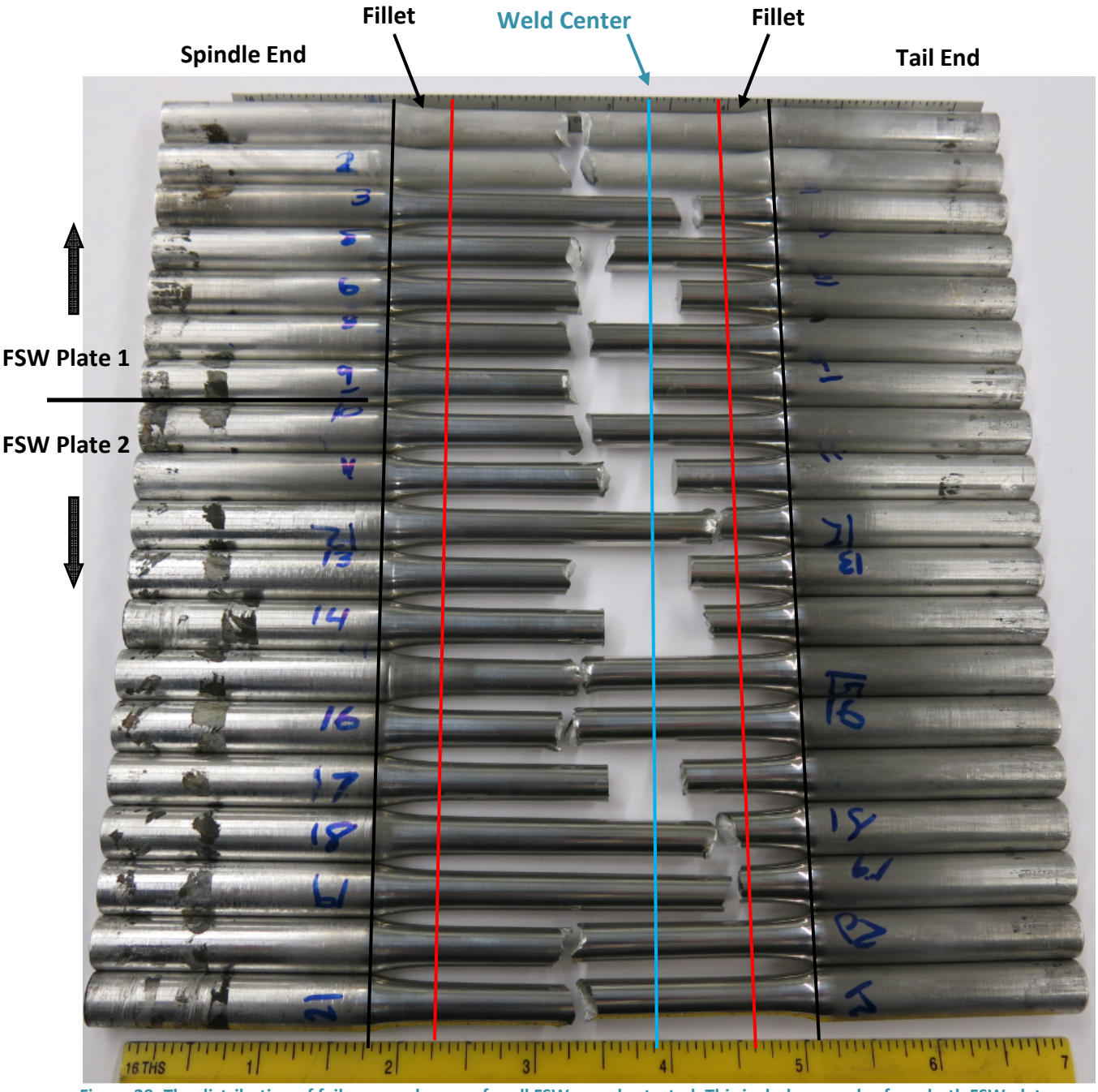

Figure 29: The distribution of failures can be seen for all FSW samples tested. This includes samples from both FSW plates and from all stress levels. Inside of the red lines is the reduced section and the blue line shows the SZ. The failures in the middle of the sample are in the retreating side and the failures on the tail of the sample are in the advancing side.

The parameters used for testing each sample, and the failure cycles for each can be seen in the testing summary table (Table VI)

Table VI: Summary Table of the Testing Conditions and Failure Locations and Cycles for all FSW Fatigue Samples

Sample	FSW Plate	Failure Side	# of Cracks	Stress (MPa)	Location of Failure	# of Cycles
FSW 1	1	Both	1	138.6	HAZ	389600
FSW 2	1	Retreating	1	138.6	HAZ	555200
FSW 3	1	Advancing	1	111.4	TMAZ/HAZ	4794400
FSW 4	1	Advancing	1	111.4	TMAZ/HAZ	7521500
FSW 5	1	Retreating	1	138.6	TMAZ/HAZ	293000
FSW 6	1	Retreating	1	127.8	TMAZ/HAZ	1066700
FSW 8	1	Retreating	1	127.8	HAZ	229400
FSW 9	1	Retreating	2	116.9	HAZ	774500
FSW 10	1	Retreating	1	111.4	HAZ	10710800
FSW 11	2	Retreating	2	122.3	TMAZ/HAZ	134000
FSW 12	2	Advancing	2	132.7	HAZ	156900
FSW 13	2	Retreating	1	116.9	HAZ	1015900
FSW 14	2	Advancing	1	122.3	TMAZ/HAZ	226800
FSW 15	2	Retreating	2	132.7	HAZ	115300
FSW 16	2	Retreating	2	111.4	HAZ	1470400
FSW 17	2	Stir Zone	2	111.4	**Stir Zone**	242800
FSW 18	2	Advancing	1	138.6	HAZ	117000
FSW 19	2	Advancing	1	111.4	HAZ	1142900
FSW 20	2	Retreating	2	122.3	HAZ	162300
FSW 21	2	Retreating	2	132.7	HAZ	82400

4.1 S-N Curve

The data gathered from fatigue testing was plotted on an S-N curve (Figure 30). There were three groups of test material: base metal 6061 and two different plates of FSW 6061. The baseline 6061 had higher fatigue strength compared to the FSW samples since failure required higher stresses at similar a number of cycles. The best metal was not able to achieve lower cycles than 10^6 because the bending required to produce enough stress for failure to occur in a shorter number of cycles would hit the shutoff switch. If the samples were able to be designed with a thicker diameter this would not be a problem. Around 5 x 10^6 cycles, the baseline 6061 was under 27 MPa more stress than the FSW samples that failed. When comparing the two FSW plates, there is a clear discrepancy between the first and second plate in fatigue strength. The plates do not have the same fatigue strength. The first plate was superior in fatigue strength since at a similar stress value of 138 MPa, FSW plate 1 had an average cycle to failure of 412,600 cycles while FSW plate 2 had failure at 117,000 cycles. This was proven statistically by fitting a Weibull cumulative failure distribution for the fatigue of both plates at 111.4 MPa (Figure 31). For each distribution, a 95% confidence interval was included (Table VII). The only place where the confidence intervals overlap is during the first 10% of failures. This means that if a group of samples from different plates are tested, 95% of the time, the average cycles to failure for each plate would not be statistically the same. Though scatter was expected in

fatigue testing, such a difference between the fatigue strength of the two plates of samples was not. The lower fatigue strength of the second plate of FSW 6061 may be attributed to weld defects such as inclusions or voids. Weld defects were likely a result of poorly optimized welding procedure that can be attributed to the prototype nature of the welding process. While most samples failed within the HAZ and TMAZ, one sample did fail in the SZ. This sample failed quickly at 242,800 cycles at only 111.5 MPa and was therefore more closely inspected later with SEM.

Compared to fatigue strength of base metal 6061 and FSW 6061 found in literature, samples produced by Sapa were stronger for both base metal and FSW. The higher fatigue strength of the material might be attributed to the processing of the aluminum, likely the extrusion, and not be taken to show that that the welds are a better quality.

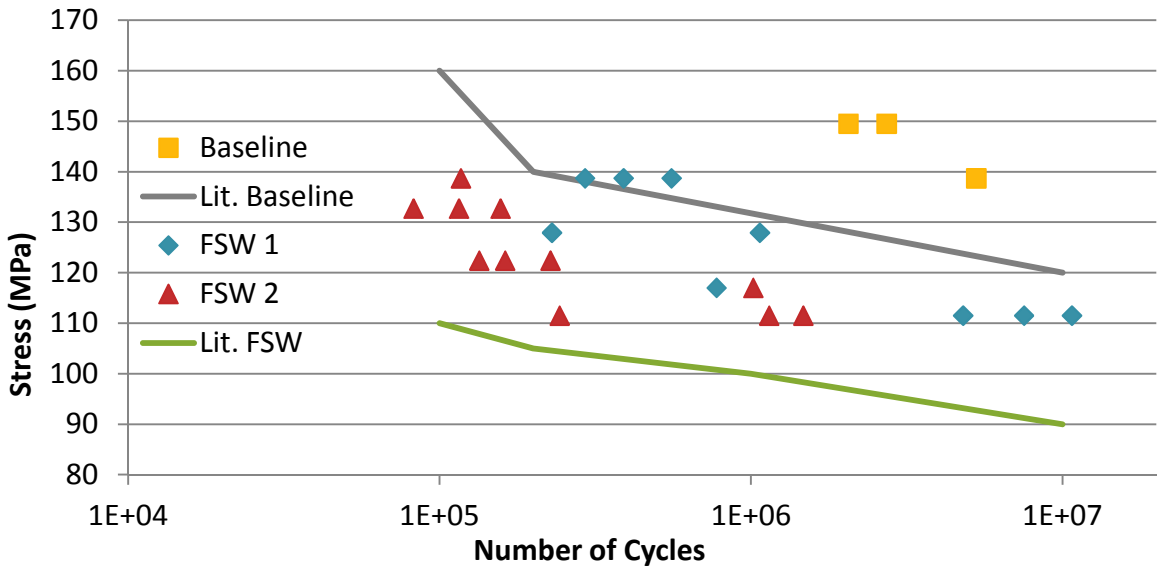

Figure 30: Stress-number of cycles to failure plot for three difference sets of samples: baseline 6061 and two plates of FSW 6061. The baseline has higher fatigue strength than the FSW samples, while FSW 1 has higher fatigue strength than FSW 2. The samples provided by Sapa had higher fatigue strength than material properties found in literature for both the baseline and FSW 6061 [32].

Table VII: α and β Parameters for Weibull Analysis (Output by JMP Statistical Software)

FSW Plate	Stress (MPa)		α	β
1	111.4	Lower 95% CI	6134172	1.9
		Estimate	8553160	3.6
		Upper 95% CI	11926067	41
2	111.4	Lower 95% CI	557455	0.91
		Estimate	1066038	1.8
		Upper 95% CI	2038617	∞
1	138.7	Estimate	454791	4.23
2	132.7	Estimate	130081.4	4.39
2	122.3	Estimate	190290	4.9

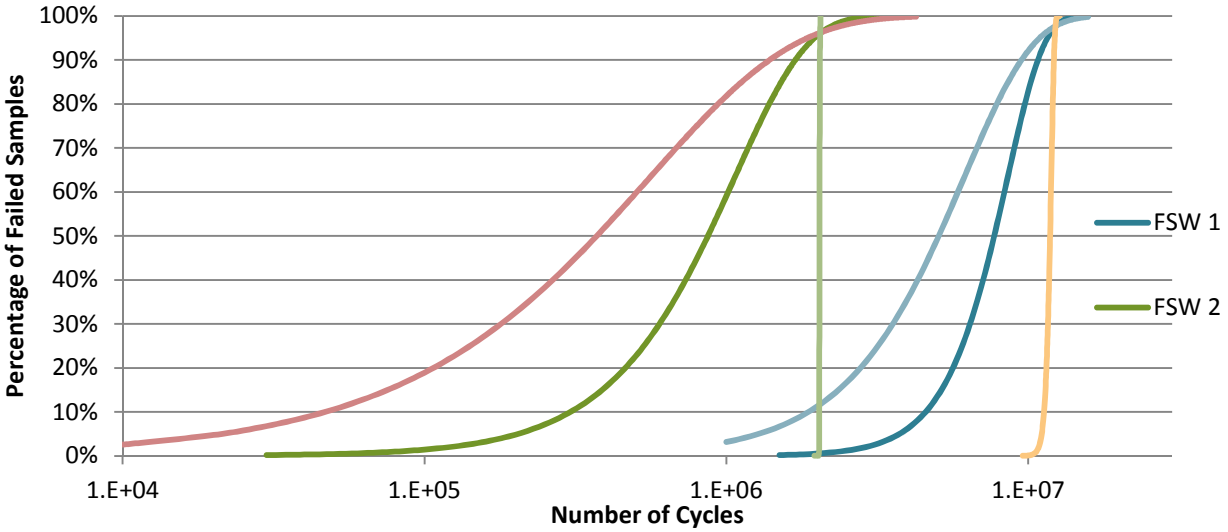

Figure 31: Cumulative failure distribution comparing the fatigue failures of plate 1 vs. plate 2 at 111.52 MPa with a confidence interval of 95%. Almost no part of the confidence intervals overlap, only below 10% where the interval is large. This shows that the FSW plates are not comparable when it comes to fatigue strength.

The failure distributions were also examined by varying the stress value of each plate. This describes the percentage of failures that occur at a specific stress after a certain number of cycles. A steeper line is ideal, meaning that 100% of the samples will fail at that given stress and none before that. The distribution should be greater at lower stresses and more vertical at higher stresses. These distributions describe the failure of the tested sample, but they should not be used to describe the population since they contain only three data points. At least seven data points are needed to have representative failure distribution.

For the first FSW plate, the distribution for the two stresses, 111.5 MPa and 138.7 MPa, were similar (Figure 32). The main difference is the longer life of the lower stress samples. The distribution only included two stress values as these were the only stresses for the first plate that had three data points.

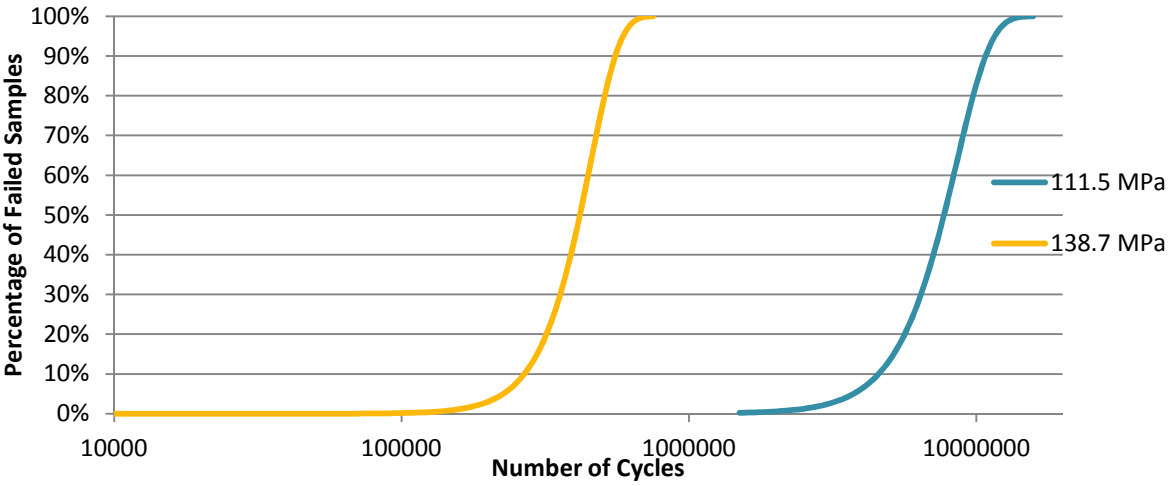

Figure 32: Cumulative distribution of failures at different stresses for the first FSW plate.

The second FSW plate had distributions that were close to the type of distributions expected (Figure 33). The lowest stress showed the largest distribution while the higher stresses had a tighter spread of data. Also the samples under a higher stress are predicted to fail sooner which is expected.

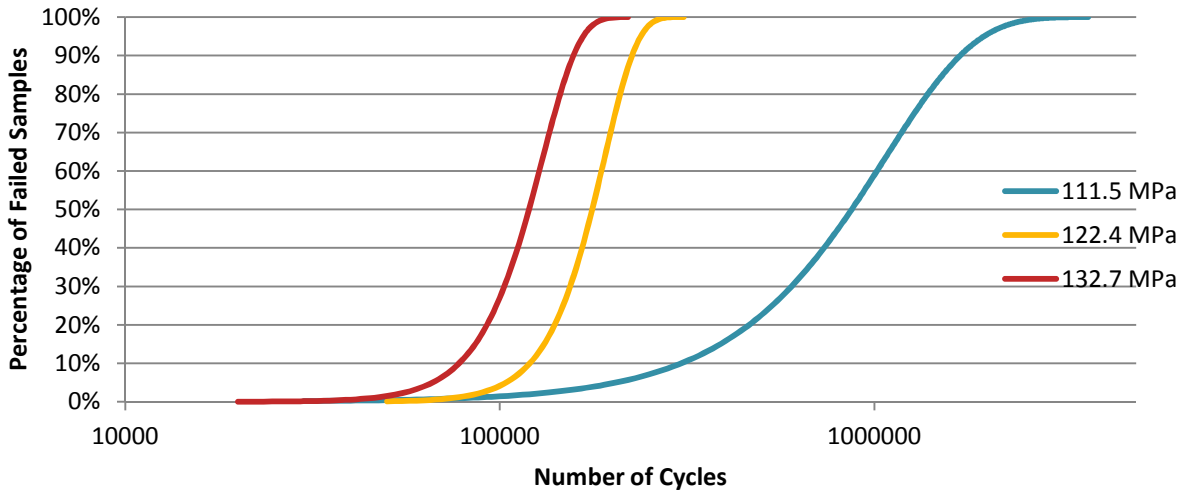

Figure 33: Cumulative distribution of failures at different stresses for the second FSW plate. For all percentages of failures, samples with more stress fail sooner. The lower stress samples also have a larger range of cycles for failure.

4.2 Failure Location

Metallography on samples was done to determine the location of failure based on the grain structure. A fractured sample was sectioned, mounted, and polished. After polishing, the macro etchant (65% nitric acid, 32% hydrochloric acid, and 3% hydrofluoric acid) was used to obtain micrographs of the different zones typical in a FSW material (Figure 34). Figure 34(a) shows the SZ with equiaxed grains. This confirms the recrystallization that occurs in the SZ. Figure 34(b) shows the TMAZ since the grains are not equiaxed and still show the effects of an extruded structure in the grains. Figure 34(c) reveals the HAZ nearing the base metal as the image was taken away from the TMAZ, but the grains were not clear with the etchant used.

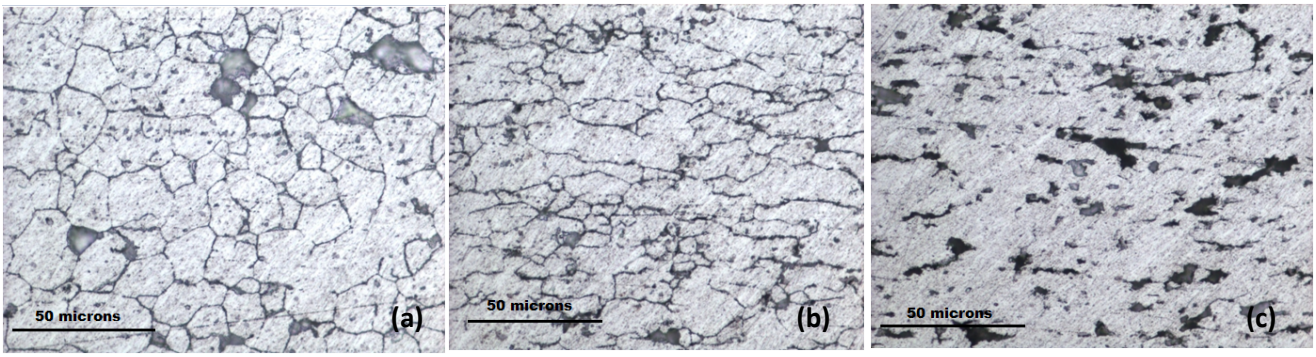

Figure 34: Micrographs of a fractured FSW 4 sample taken at 500x magnification. (a) SZ, (b) TMAZ, (c) HAZ.

A micrograph of the fracture and the structure around it shows the resemblance of the structure in the HAZ (Figure 35). This sample failed in the HAZ. Most failures during testing occurred in similar areas either a little farther in the HAZ or closer to the TMAZ.

Figure 35: Micrograph of fracture taken at 200x magnification. Structure resembles that of the HAZ

To verify the failure location, a hardness profile was produced for four different samples: samples 4, 6, 13, and 14 (Figure 36). Microhardness measurements were taken beginning from the stir zone towards the crack at 20/1000^{ths} of an inch increments with 500 grams force using the Vickers microhardness diamond indenter. Samples 4, 6, and 14 failed at low hardness values outside of the stir zone. Failure ranged from the region of falling hardness in the TMAZ to areas into the HAZ on the opposite side of the lowest hardness region as shown in Figure 20. Sample 13 was the only sample that failed as hardness was increasing, from a low point of 63 HV to 76 HV, which indicates that the failure occurred farther into the HAZ and close to the base metal as the hardness increased. Samples 4, 6, and 14 all failed closer to the TMAZ/HAZ boundary.

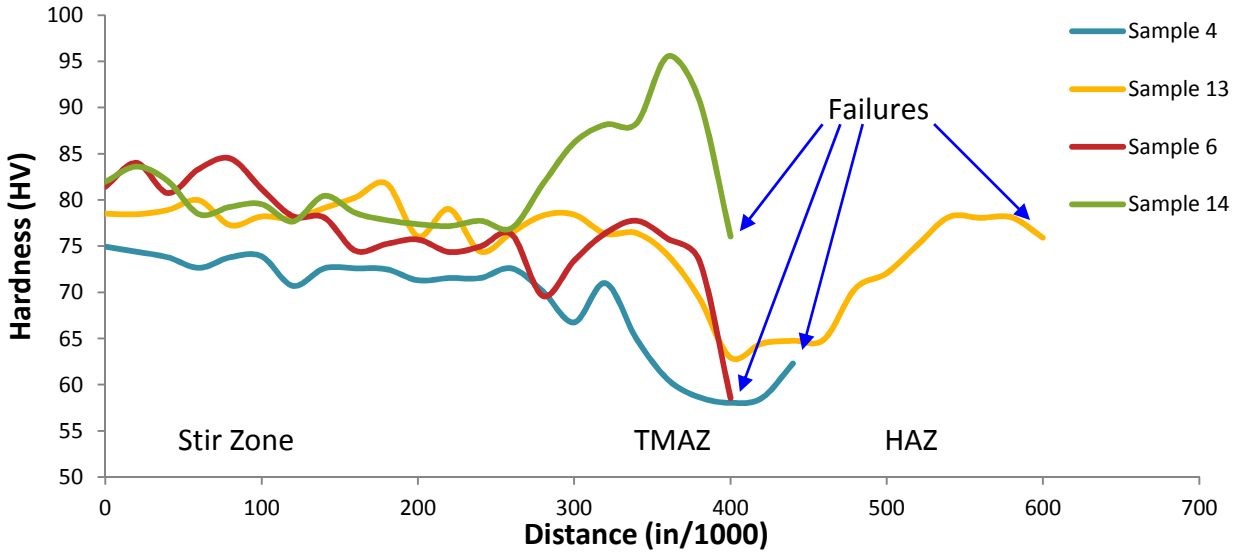

Figure 36: Hardness profile of four failed samples starting in the SZ. Sample 6 and 14 both failed as hardness was dropping while sample 4 and 13 failed while hardness recovers, where sample 13's hardness recovers more than sample 4's hardness.

4.3 Fracture Surface Analysis

Scanning electron microscopy (SEM) was done to examine the fracture surface of three FSW samples: samples 9, 11, and 17. The surfaces had multiple distinct regions: ductile and brittle regions, as well as smooth regions where cracks likely started. Some of these samples had cracks on two sides, which is not uncommon for RBF fatigue. If the samples were wobbling during testing this was less likely. Sample 9 had two cracks, brittle regions, on either side of the sample and a ductile region in the center between the two cracks (Figure 37). On the right side crack, a smooth section with an abnormality was found. Upon closer inspection, a valley was seen that reaches the edge of the sample and may have been a weak point where crack initiated. Striations cannot be seen in these samples as the crack progressed through the cross section. Since the samples had multiple cracks, the surfaces would rub together when the opposite crack was in tension. After many cycles, this wear erased the striations that had formed due to crack propagation.

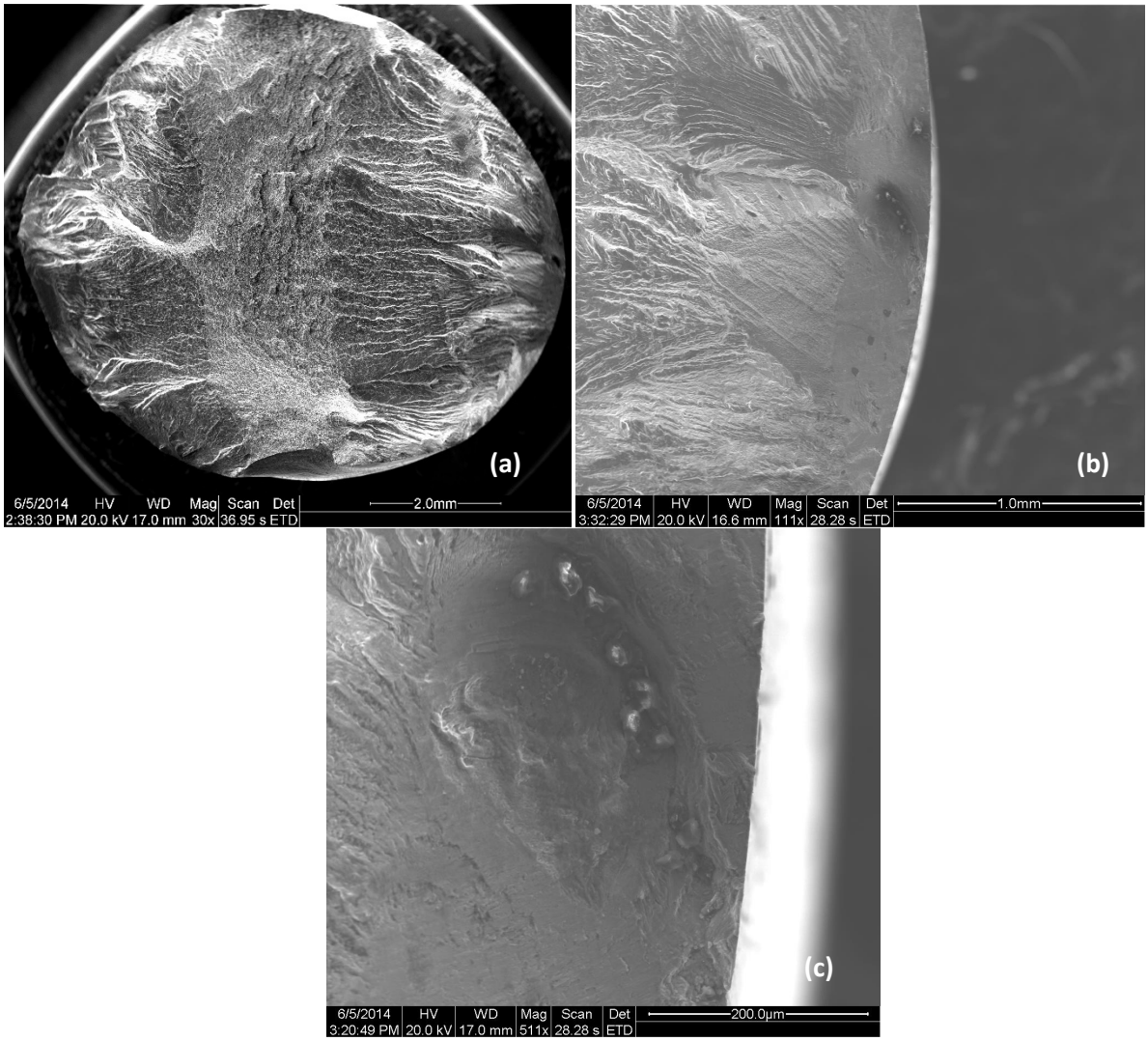

Figure 37: Fracture surface of sample 9. (a) Overall view of sample. (b) Close up of area where crack is thought to have initiated. (c) More zoom into smooth area where crack may have started shows a valley that reaches to the surface that could have caused sample to fail.

The second sample that was looked at under the SEM was sample 11, a sample from the second FSW plate (Figure 38). This sample shows multiple cracks: one from the left side and another form the right side. The ductile region is located between the left side crack and the right side crack. There were few visible abnormalities on this sample.

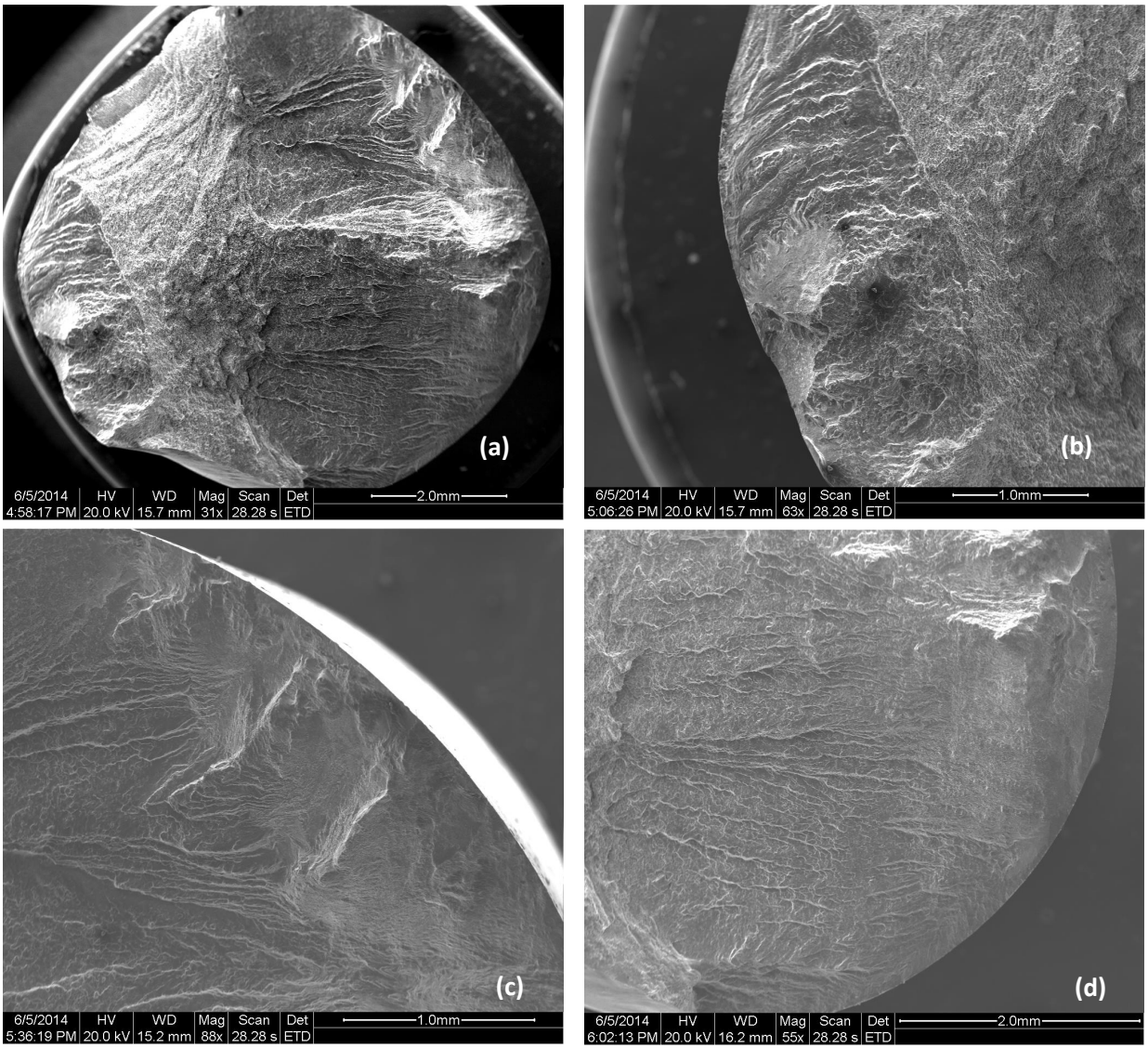

Figure 38: Fracture surface of sample 11. (a) Overall view of sample 11 that shows multiple cracks. (b) Crack propagating from left side. (c) Crack propagating from top right corner. (d) Crack propagating from bottom left corner.

The final sample viewed in the SEM was sample 17, the sample that failed in the stir zone and not in the HAZ or TMAZ like all the other samples (Figure 39). The surface of this sample was different than the previous samples since it failed in a different region. Even the brittle and ductile regions looked different. It was also difficult to find where a crack began or if there were

multiple cracks. Like the other samples, the smooth regions may be where the cracks began. Upon closer inspection (Figure 39 (d)), it was found that the wave like ridges were the ductile regions and smooth areas around the edges of the sample were the brittle regions. Throughout the sample, there were several dark spots that revealed particles that stood out from the surface when the magnification was increased. These particles may be inclusions that could have led to the weakened stir zone and caused failure to occur in an unexpected location. Along with the particles, there were holes that may be voids that also contributed to the early failure and failure in the stir zone.

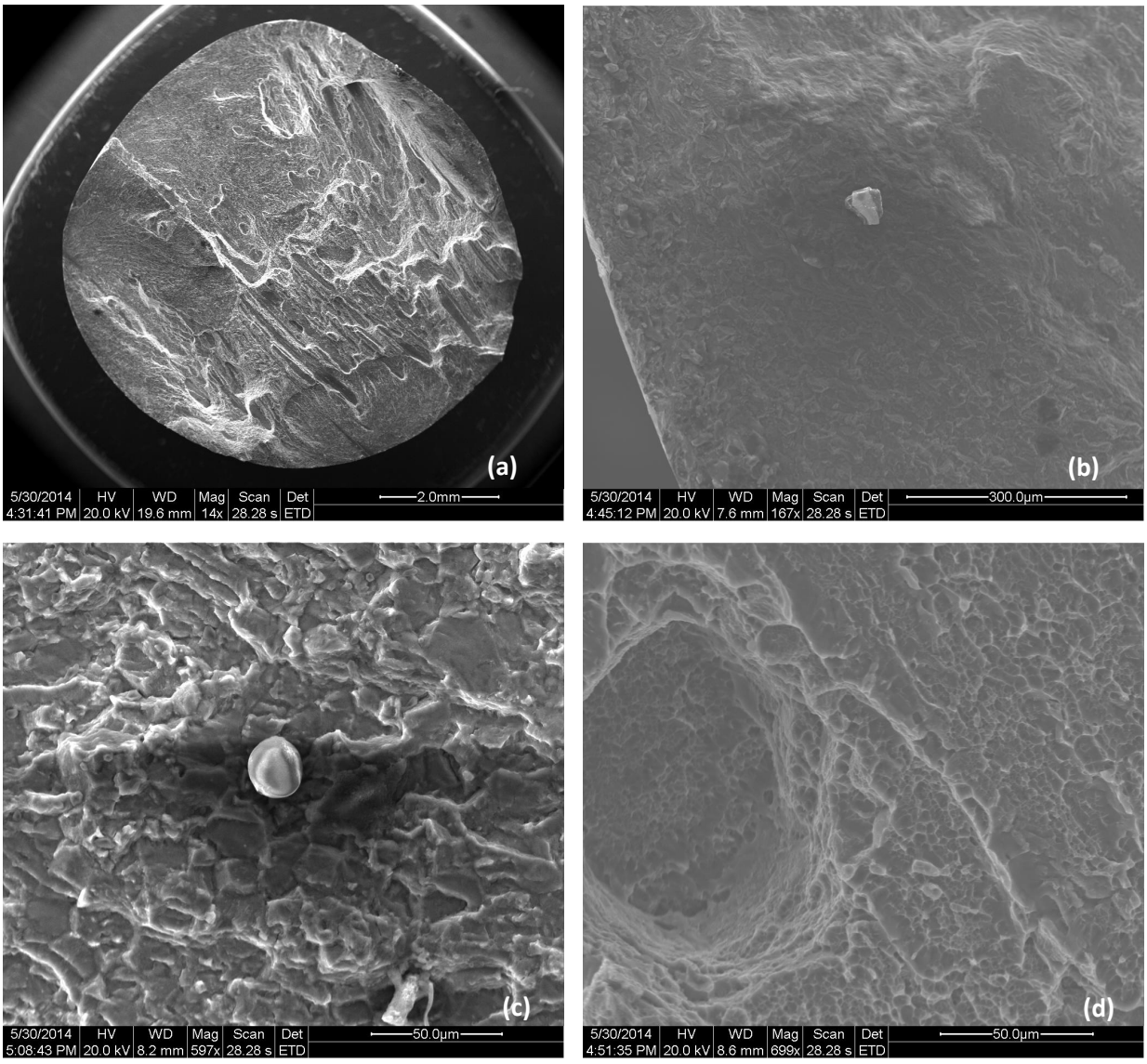

Figure 39: Fracture surface of sample 17 where sample failed in the SZ. (a) Overall view of sample. (b) Particulate that stands out from the rest of the surface close to the edge of sample in the lower left side. (c) Small inclusion in a dark spot of the surface on the upper section of the sample. (d) Ductile region with a possible void.

5 Conclusions

The fatigue strength of FSW 6061-T6 aluminum is lower than that of base 6061-T6 aluminum. Both base metal and FSW material from Sapa had greater fatigue strength than seen in literature likely due to the processing involved in making the aluminum plates. The fatigue strength at 5 million cycles for a sample from FSW 1 compared to base metal 6061-T6 was 27 MPa less. The weaker fatigue strength in FSW 6061 can be tied to the weakening of the material from the welding process shown with the hardness profile where the weakest point is 0.5 inches from the center of the weld between the HAZ and TMAZ. The characteristic life of FSW plate 1 was 8,553,160 cycles at 111.4 MPa and 454,791 cycles at 138.7 MPa. The characteristic life of FSW plate 2 was 1,066,038 cycles at 111.4 MPa. The second FSW plate had lower fatigue strength compared to the first FSW plate due to weld defects from poorly optimized prototype welding process. Metallography and microhardness showed that most samples failed in the HAZ and TMAZ based on the structure and hardness at the fracture location. Most FSW samples failed in these zones except for one sample that failed in the SZ. When the sample that failed in the SZ was inspected with the SEM, multiple inclusions and voids were found that likely led an early failure as well as failure in the zone that should have been stronger due to recrystallization of the grains.

6 References

[1] J. Hilgert, "Knowledge Based Process Development of Bobbin Tool Friction Stir Welding," Helmholtz-Zentrum Geesthacht, Germany, 2012.

[2] "Properties of Wrought Aluminum and Aluminum Alloys, Properties and Selection: Nonferrous Alloys and Special-Purpose Materials," *ASM Handbook,* vol. 2, pp. 62-122, 1990.

[3] *CES EduPack,* Granta Design, 2013.

[4] "How and Why Alloying Elements are Added to Aluminum," ESAB, [Online]. Available: http://www.esabna.com/us/en/education/knowledge/qa/How-and-why-alloying-elements-are-added-to-aluminum.cfm. [Accessed 1 January 2014].

[5] "Aluminum-Magnesium-Silicon (6000) Alloys," [Online]. Available: http://www.keytometals.com/article74.htm. [Accessed 20 January 2014].

[6] D. J. Chakrabarti and D. E. Laughlin, "Phase Relations and Precipitation in Al-Mg-Si alloys with Cu Additions," *Progress in Materials Science,* no. 49, pp. 389-410, 2004.

[7] A. H. Feng, D. L. Chen and Z. Y. Ma, "Microstructure and Low-Cycle-Fatigue of a Friction-Stir-Welded 6061 Aluminum Alloy," *Metallurgical and Materials Transactions A,* vol. 41A, pp. 2626-2641, 2010.

[8] "Heat Treating of Aluminum Alloys, Heat Treating," *ASM Handbook,* vol. 4, pp. 841-879, 1991.

[9] "Metal Extrusion," [Online]. Available: www.thelibraryofmanufacturing.com/extrusion.html#top.

[10] W. F. Smith and J. Hashemi, "Fatigue," in *Foundations of Materials Science and Engineering*, New York, McGraw Hill, 2010, pp. 291-298.

[11] "Non-Ferrous Extrusions," [Online]. Available: www.non-ferrous.com/website/aluminum-information/#extrusions.

[12] T. Chanda, J. Zhou and J. Duszczyk, "A Comparative Study on Iso-Speed Extrusion and Isothermal Extrusion of 6061 Al Alloy Using 3D FEM Simulation.," *Journal of Materials Processing Technology,*

no. 114, pp. 145-153, 2001.

[13] L. D, S. M, D. F and P. T, "Linking Microstructure and High Temperature Ductility in Aluminum Alloys AA6xxx," *Université catholique de Louvain.*

[14] C. C. Flake, "Elements of Metallurgy and Engineering Alloys: Fatigue," *Elements of Metallurgy and Engineering Alloys,* no. ASM International, 2008.

[15] "High Cycle Fatigue," efunda, [Online]. Available: http://www.efunda.com/formulae/solid_mechanics/fatigue/fatigue_highcycle.cfm. [Accessed 24 January 2014].

[16] M. R. Mitchell, "Fundamentals of Modern Fatigue Analysis for Design," *Rockewell Science Center.*

[17] N. E. Nanninga, "High Cycle Fatigue of AA6082 and AA6083 Aluminum Extrusions," Michigan Technological University, 2008.

[18] J. J. Xiong and R. Shenoi, Reliability and Confidence Intervals of Fatigue Life: Fatigue and Fracture Reliability Engineering, London: Springer, 2011.

[19] P. S. Veers, "Statistical Considerations in Fatigue: Fatigue and Fracture," *ASM Handbook,* vol. 19, pp. 295-302, 1996.

[20] R. B. Abernethy, "An Overview of Weibull Analysis," *The New Weibull Handbook,* pp. 1-10.

[21] P. M. G. P. Moreira, A. M. P. De Jesus, A. S. Ribeiro and P. M. S. T. De Castro, "Fatigue Crack Growth in Friction Stir Welds of 6082-T6 and 6061-T6 Aluminum Alloys: A Comparison," University of Porto.

[22] R. K. Shukla and P. K. Shah, "Comparative Study of Friction Stir Welding and Tungsten Inert Gas Welding Process," *Indian Journal of Science and Technology,* vol. 3, no. 6, pp. 667-671, 2010.

[23] S. W. Kallee, "Friction Stir Welding in Series Production," *Automobil Production,* 2004.

[24] P. Staron, M. Kocak and S. Williams, "Residual Stresses in Friction Stir Welded Al Sheets," *Applied Physics A: Materials Science and Processing,* no. 74, pp. 1161-1162, 2002.

[25] M. Ericsson and R. Sandstrom, "Influence of Welding Speed on the Fatigue of Friction Stir Welds, and Comparison with MIG and TIG," *International Journal of Fatigue,* vol. 25, pp. 1379-1387, 2003.

[26] M. Guerra, C. Schmidt, J. C. McClure, L. E. Murr and A. C. Nunes, "Flow Patterns During Friction Stir Welding," *Materials Characterization,* vol. 49, pp. 95-101, 2003.

[27] K. K. Ramachandran, "An Introduction to Friction Stir Welding," Engineering College Thrissur.

[28] T. R. McNelley, S. Swaminathan and J. Q. Su, "Recrystallization mechanisms during frcition stir welding/processing of aluminum alloys," *Scripta Materiala,* vol. 58, pp. 349-354, 2008.

[29] P. Moreira, M. de Figueiredo and P. de Castro, "Fatigue Behavior of FSW and MIG Weldments for Two Aluminum Alloys," *Theoretical and applied fracture mechanics,* vol. 48, pp. 169-177, 2007.

[30] P. Singh, S. K. Gandhi and H. Shergill, "Comparative Study of Friction Stir and TIG Welding for Aluminum 6063-T6," *INternational Journal of Engineering Research & Technology,* vol. 1, no. 10, 2013.

[31] P. L. Threadgil, M. M. Z. Ahmed, J. P. Martin, J. G. Perrett and B. P. Wynne, The Use of Bobbin Tools for Friction Stir Welding of Aluminum Alloys, Berlin: Thermec, 2009.

[32] Y. Uematsu, K. Tokaji and H. Shibata, "Fatigue Behavior of Friction Stir Welded 6061-T6 Aluminum Alloys".